

# Low-input lipidomics reveals lipid metabolism remodelling during early mammalian embryo development

Received: 27 August 2022

Accepted: 20 December 2023

Published online: 01 February 2024

 Check for updates

Ling Zhang<sup>1,2,12</sup>, Jing Zhao<sup>1,2,12</sup>, Sin Man Lam<sup>3,4,12</sup>, Lang Chen<sup>1,12</sup>, Yingzhuo Gao<sup>5,6,12</sup>, Wenjie Wang<sup>1,12</sup>, Yuyan Xu<sup>1</sup>, Tianyu Tan<sup>1</sup>, Hua Yu<sup>1</sup>, Min Zhang<sup>1</sup>, Xufeng Liao<sup>1</sup>, Mengchen Wu<sup>1</sup>, Tianyun Zhang<sup>2</sup>, Jie Huang<sup>7</sup>, Bowen Li<sup>4</sup>, Quan D. Zhou<sup>8</sup>, Ning Shen<sup>10</sup>, Hyeon Jeong Lee<sup>10</sup>, Cunqi Ye<sup>10</sup>, Da Li<sup>10</sup>, Guanghou Shui<sup>1,3,10</sup> & Jin Zhang<sup>1,2,11</sup>

Lipids are indispensable for energy storage, membrane structure and cell signalling. However, dynamic changes in various categories of endogenous lipids in mammalian early embryonic development have not been systematically characterized. Here we comprehensively investigated the dynamic lipid landscape during mouse and human early embryo development. Lipid signatures of different developmental stages are distinct, particularly for the phospholipid classes. We highlight that the high degree of phospholipid unsaturation is a conserved feature as embryos develop to the blastocyst stage. Moreover, we show that lipid desaturases such as SCD1 are required for *in vitro* blastocyst development and blastocyst implantation. One of the mechanisms is through the regulation of unsaturated fatty-acid-mediated fluidity of the plasma membrane and apical proteins and the establishment of apical–basal polarity during development of the eight-cell embryo to the blastocyst. Overall, our study provides an invaluable resource about the remodelling of the endogenous lipidome in mammalian preimplantation embryo development and mechanistic insights into the regulation of embryogenesis and implantation by lipid unsaturation.

After mammalian fertilization of an oocyte by a sperm, the totipotent zygote undergoes three to four rounds of cell division followed by compaction at the eight-cell stage. This then forms the morula, which differentiates into the blastocyst that contains inner cell mass (ICM) and outer layer trophectoderm (TE) cells<sup>1</sup>. These processes depend on maternal RNA and protein degradation and resynthesis<sup>2</sup>, epigenetic reprogramming and chromatin structure organization<sup>3–6</sup>. The dynamic transitions are associated with metabolic reprogramming in which early-cleavage-stage embryos remain in a quiescent state that requires pyruvate and lactate and then transition into a highly oxidative state that needs glucose to support blastocyst development<sup>7,8</sup>.

Importantly, metabolites play key roles in development and cell fate decisions, such as pyruvate, which is indispensable for zygote genome activation<sup>9</sup>, and glucose, which distinguishes the cell fate of TE and ICM cells<sup>8</sup>. The metabolomic profiling of early embryos identified L-2-hydroxyglutarate as a highly abundant metabolite in oocytes, the depletion of which facilitated histone mark erasure after fertilization<sup>10</sup>. However, less attention has been given to lipid metabolism and its impact on mammalian preimplantation embryo development.

Lipids have essential roles in energy production<sup>11</sup>, differentiation<sup>12</sup>, proliferation and signalling<sup>13</sup>. Previous studies have shown that lipid remodelling occurs in the development of invertebrate animals such

as *Drosophila melanogaster*<sup>14</sup>. A study of the lecithotrophic organism zebrafish revealed dynamic compositions of lipid species in the yolk and body during embryogenesis<sup>15</sup>. Previous studies of endogenous fatty acids and triglycerides of oocytes have revealed that beta-oxidation has an essential role in energy metabolism for oocyte maturation and development<sup>16–21</sup>. And studies of in vitro-cultured bovine embryos have revealed categories of lipids during mammalian embryogenesis<sup>22</sup>. However, a global picture of various categories of lipids in mouse and human embryos in vivo is missing. Imaging technologies have been adopted to observe lipids<sup>23–25</sup>, which enable us to visualize lipid droplet (LD) distribution<sup>24</sup> and to study the importance of LD size, synthesis and maintenance during mouse embryo development<sup>26,27</sup>. Moreover, exogenous supply of fatty acids in culture medium can affect oocyte maturation, cryopreservation, oxidative stress and cellular signalling in a variety of species<sup>28–30</sup>, and supplementation of saturated fatty acid can lead to endoplasmic reticulum (ER) stress<sup>31–37</sup>. These results highlight the important and complex roles of lipids during oocyte and early embryo development. But the full landscape of lipid remodelling and through what mechanisms it can contribute to physiological embryo development before and during implantation remains elusive. Thus, we sought to provide a comprehensive lipid remodelling landscape using systematic lipidomics approaches to analyse mammalian preimplantation embryo development. We identify a previously neglected metabolic regulation pathway for the degree of lipid unsaturation, membrane fluidity and apical–basal polarity establishment in mouse early embryo development and in the formation of cultured blastoids.

## Results

### Stage-specific lipidomics signatures during mouse preimplantation embryo development

To study the lipid remodelling process in early mouse embryo development, we first evaluated the sensitivity of our lipidomics method with a small number of embryo samples. Based on the range of our recently optimized ultralow-input metabolomics approach<sup>10</sup>, we first used 120 zygotes and 120 two-cell embryos to test the number needed for lipidomics. Endogenous lipids that were clearly detected and enriched in biological samples relative to blank samples were obtained. Overall, 221 lipid species from 22 major classes could be quantified using appropriate deuterated internal standards specific to each lipid class (Extended Data Fig. 1a). We subsequently used this high-coverage targeted lipidomics approach to profile dynamic lipid remodelling in mouse oocytes and preimplantation embryos. Specifically, 120 metaphase II (MII) oocytes, zygotes and two-cell, four-cell, eight-cell and blastocyst stage embryos were collected at the indicated times. Then an isopropanol (IPA)-based extraction method followed by high-performance liquid chromatography with mass spectrometry (HPLC–MS) were performed (Fig. 1a). Principal component analysis (PCA) showed that even though there was inter-group variance, samples for each stage were clustered together and separate from the others (Fig. 1b and Supplementary Table 1), which indicated that different embryonic stages exhibit distinct lipidomics signatures. In particular, the blastocyst stage was more markedly separated from all other stages, which suggested that there was a major shift in lipid composition during this period compared with the other developmental periods. A total of 332 lipid species from 23 classes were detected (Fig. 1c), which comprised glycerophospholipids (phospholipids, plasmalogen phospholipids and lysophospholipid), glycerolipids (diacylglycerols (DAGs) and triacylglycerols (TAGs)), sphingolipids (sphingomyelins (SMs) and ceramides (Cers)) and cholesterol<sup>38</sup>. A detailed analysis showed that the proportional abundance of individual lipid species dynamically changed during development (Extended Data Fig. 1b,c). We then applied the method maSigPro<sup>39</sup> to identify different trends of lipid clusters along the six developmental stages. In total, we observed five distinct lipid clusters representing different trends of regulation (Extended Data Fig. 1d,e). Among these, cluster 1 consisted of lipids that were reduced during development,

mainly including phosphatidylethanolamines (PEs) and phosphatidylinositol (PIs), which indicated that enrichment of these lipids might be important for oocyte activation and fertilization. Cluster 2 represented lipids that are abundant in oocytes, depleted after fertilization and gradually repleted in the blastocyst stage. Long-chain fatty acid phosphatidylcholines (PCs) dominated this cluster, and considering that they are a major component of the plasma membrane, their enrichment in the blastocyst stage implies that there is dynamic membrane remodelling during this period. Cluster 3 represented lipids that are more specifically required in the blastocyst stage. In addition to certain PCs, this cluster included SMs that might be crucial for microdomain formation on the membrane to support signalling molecule distribution. Cluster 4 and cluster 5 included lipids that gradually emerge from the four-cell stage or even the two-cell stage, which suggested that biosynthesis of certain types of nascent lipids takes place immediately after zygote genome activation. Overall, the Shannon diversity index<sup>40</sup>, which measures the evenness of species in a group, showed an increasing trend from the oocyte and zygote stages to the blastocyst stage. This result indicates that the pool of different lipid species becomes more diverse and evenly distributed along the developmental process (Fig. 1d), probably to accommodate the increasingly complicated biological processes.

We used a second method, Bligh&Dyer extraction, to validate these results using the same number of embryos per replicate of all developmental stages. Bligh&Dyer extraction effectively recovers both phospholipids and neutral lipids<sup>41</sup>, and we obtained highly consistent global patterns of lipidomics remodelling data (Extended Data Fig. 2a and Supplementary Table 2). The lipid signature at the blastocyst stage was clearly separated from the other embryo stages (Extended Data Fig. 2a). It also revealed high levels of phospholipid components, such as PCs, and neutral lipid components, such as TAGs and cholesterol, across the embryo development stages (Extended Data Fig. 2b–d). Together, these results demonstrate that we were able to generate high-quality lipidomics data for both phospholipids and neutral lipids during mouse early embryo development.

### Dynamic changes in individual lipid classes during mouse preimplantation embryo development support various lipid-mediated functions

To understand the dynamic changes and functions of each lipid class during preimplantation development, the abundance of individual lipid classes were separately analysed. Glycerophospholipids are the main components of the cell membrane, including PCs, PEs, PIs, phosphatidylserines (PSs) and cardiolipins (CLs). The most predominant one was PCs and, notably, its abundance exhibited a bimodal distribution, with higher levels at the oocyte and blastocyst stages. Moreover, longer and unsaturated fatty acyl chains (PC38–PC42) were enriched at the blastocyst stage (Fig. 2a). PEs exhibited a steady reduction in abundance from oocytes and, unlike PCs, they were not repleted at the blastocyst stage (Fig. 2b). This result was consistent with cell membrane PE staining by duramycin, which binds PEs with high specificity and affinity (Extended Data Fig. 3a). PCs and PEs primarily reside in the outer leaflet and inner leaflet of the plasma membrane; therefore, these results suggested that there is dynamic remodelling of membrane components during development. Notably, the plasmalogen phosphatidylcholines (PC Os) comprising polyunsaturated fatty acids (PUFAs) were markedly increased in abundance at the blastocyst stage (Fig. 2c), whereas the majority of plasmalogen phosphatidylethanolamines (PE Os) decreased in abundance, except for a few highly unsaturated species, such as PE O-38:7(O-16:1\_22:6) and PE O-38:6(O-16:1\_22:5), which contain docosahexaenoic acid and docosapentaenoic acid, respectively (Fig. 2d). Plasmalogen is associated with cholesterol homeostasis<sup>42–44</sup>, which influences cell membrane fluidity<sup>45</sup>. It is also a potential antioxidant owing to its high level of PUFAs<sup>46</sup>. Thus, the dynamic patterns of PC Os and PE Os suggest that they have a role in maintaining cholesterol

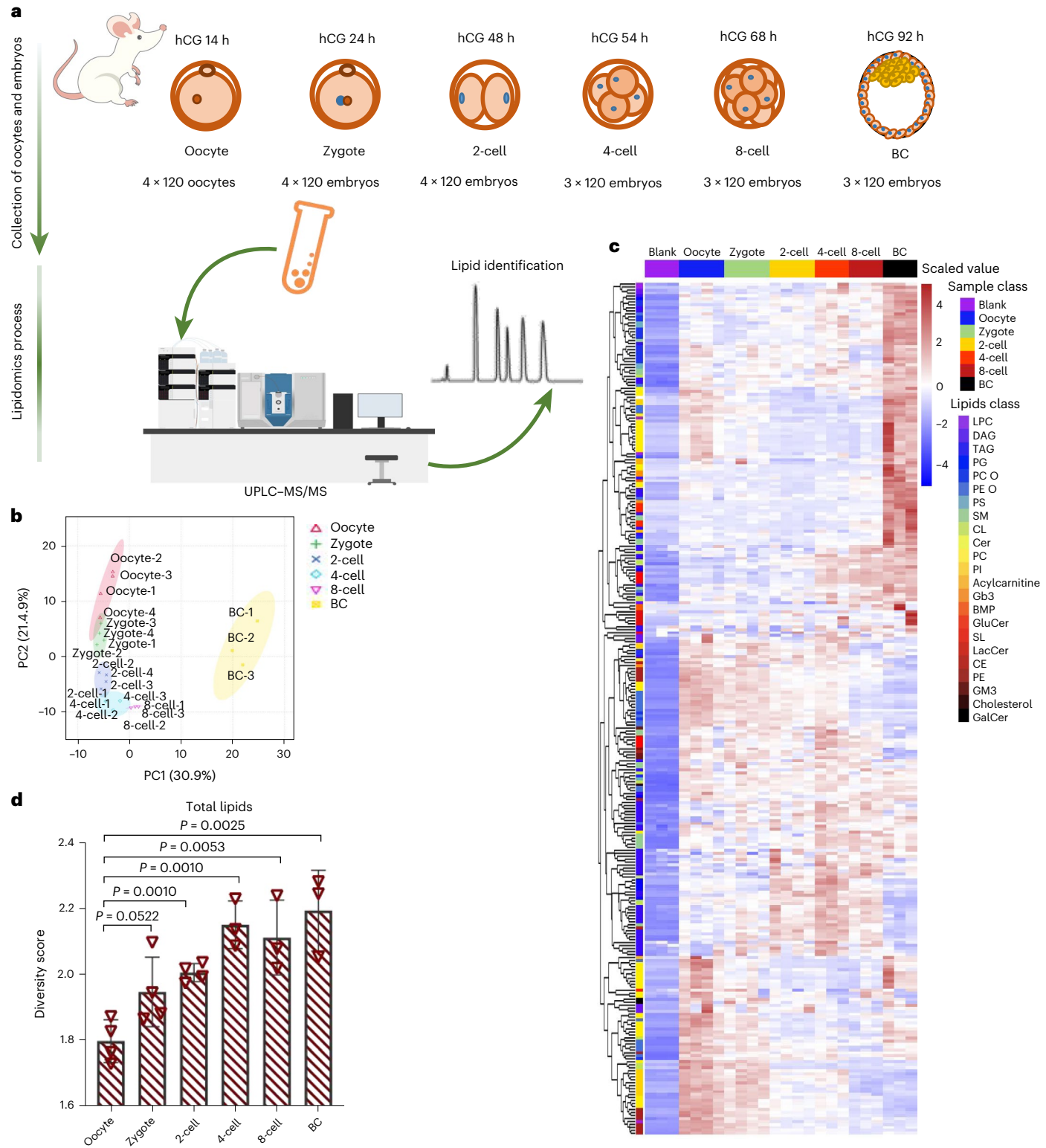
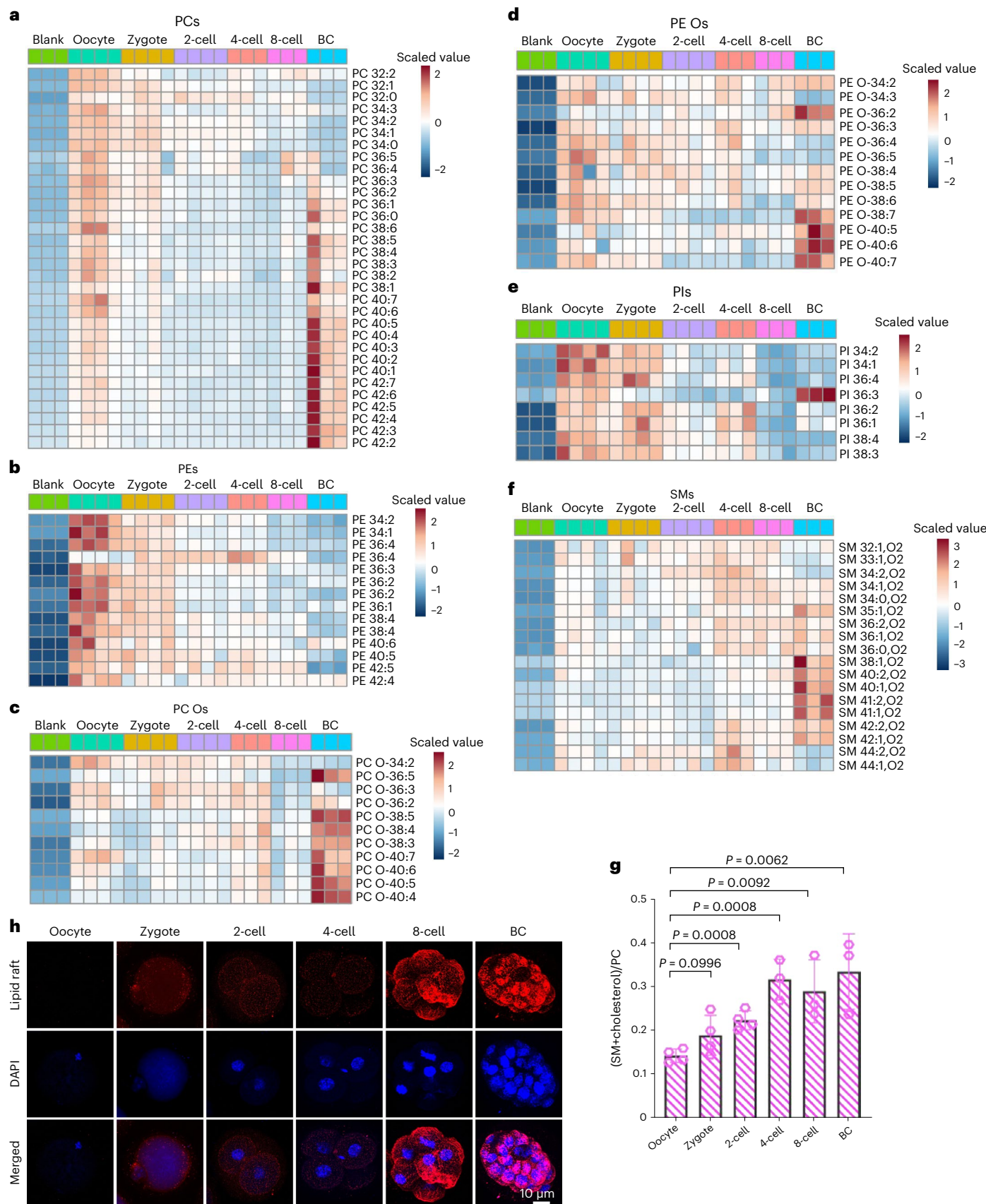


**Fig. 1 | Stage-specific lipidomics signatures in mouse preimplantation embryo development.** **a**, Schematic workflow of embryo collection and lipidomics experiments. hCG, human chorionic gonadotrophin; UPLC–MS/MS, ultra-performance liquid chromatography with tandem mass spectrometry.

**b**, A PCA plot of the lipidomics profiling data showing clustering of four biological replicates of oocytes, zygote and two-cell stage embryos each and three biological replicates of four-cell, eight-cell and blastocyst (BC) stage embryos each.

**c**, Heatmap showing the relative abundance of lipids in the six

developmental stages. Scaled value bar indicates the relative concentration. Data are from the same biological replicates as in **b**. PG, phosphatidylglycerols; LacCer, lactosylceramides; CE, cholesteryl esters; GM3, monosialogangliosides; GalCer, galactosylceramides. **d**, Diversity scores were calculated to estimate the diversity of lipid species in each developmental stage. Each dot represents one biological replicate, data are from the same biological replicates as in **b** and are presented as the mean  $\pm$  s.e.m. Statistical significance was determined by two-tailed unpaired *t*-test.



homeostasis, membrane fluidity and the redox environment to support embryo development.

Next, we examined the class of PIs. Levels were the highest in oocytes and zygotes and gradually decreased through

development until the eight-cell and blastocyst stages (Fig. 2e). PIs can function as signalling molecules<sup>47</sup>, and in oocyte development, inositol 1,4,5-trisphosphate can recognize and bind the inositol 1,4,5-trisphosphate receptor on the surface of the ER membrane, which

**Fig. 2 | Dynamic changes in the contents of individual lipid classes during mouse preimplantation embryo development support lipid-mediated functions.** **a–f**, Heatmaps showing the abundance of each class of species of PCs (**a**), PEs (**b**), PC Os (**c**), PE Os (**d**), PIs (**e**) and SMs (**f**) in the six developmental stages. Scaled value bar indicates the relative concentration. Data are from four biological replicates of oocytes, zygote and two-cell stage embryos each and three biological replicates of four-cell, eight-cell and blastocyst stage

leads to release of  $\text{Ca}^{2+}$  into the cytosol and promotion of oocyte activation after fertilization<sup>48</sup>. The high abundance of PI in oocytes and zygotes agrees with this role of PIs in oocyte activation.

The majority of the CL species were enriched along development (Extended Data Fig. 3b). Most of the very long fatty-acid chain CLs were enriched from the four-cell stage and eight-cell stage to the blastocyst stage. CLs are located in the inner membrane of mitochondria to maintain mitochondrial integrity and functions in respiratory supercomplex formation, cristae biogenesis and the tricarboxylic acid cycle<sup>49</sup>, and its deficiency results in disrupted mitochondrial morphology and defective functions<sup>50</sup>. The increased CL content is consistent with increased mitochondrial functions such as oxidative phosphorylation during preimplantation embryo development<sup>10</sup>.

Sphingolipids, mainly consisting of Cers, SMs and glycosphingolipids, form specialized microdomains on the cell membrane and promote signal transduction. SMs with cholesterol is not only an essential cellular structure component for lipid rafts but also required for cell division and differentiation<sup>51</sup>. Our results showed that most SM species became more enriched towards the blastocyst stage (Fig. 2f), and the ratio of (SM+cholesterol)/PC, which indicates raft microdomains<sup>52</sup>, was increased during the process (Fig. 2g). This result was in line with lipid raft staining of live embryos (Fig. 2h), which suggests that the formation of lipid rafts is increased to accommodate signal transduction molecules on the embryo cell surface during development. Notably, we found that the pattern of changes for the phospholipids such as PCs and PIs and for the sphingolipids such as SMs and glucosylceramides (GluCers) were highly consistent between the IPA method (Fig. 2 and Extended Data Fig. 3) and the Bligh&Dyer method (Extended Data Fig. 4a–f). Because the Bligh&Dyer method is better for recovery of neutral lipids, we analysed TAGs using this method. We found a steady increase in TAGs with altered constituent acyl chain components from the two-cell stage during the developmental process (Extended Data Fig. 4g). Specifically, TAG species with fatty-acid chain lengths of total carbon atom numbers 50–56 peaked at the 4-cell and 8-cell embryos, whereas those with chain lengths of 54–56 peaked at the blastocyst stage. TAGs are the major component of LDs, the conventional function of which is energy storage in metabolic tissues. Embryos depleted of LDs fail to develop to the blastocyst stage or survive during diapause<sup>27,53</sup>,

embryos each. **g**, The ratio of (SM+cholesterol)/PC, which indicates the level of lipid rafts in the six developmental stages. Each dot represents one biological replicate, data are from the same biological replicates as in **a** and are presented as the mean  $\pm$  s.e.m. Statistical significance was determined by two-tailed unpaired *t*-test. **h**, Staining of lipid rafts showing their formation during embryo development.

which indicates that LDs have important roles in vertebrate embryonic development. The steady increase in TAGs is probably to support the increasing demand of energy and biosynthesis, such as producing the membrane components<sup>10</sup>.

Together with the two different methods, we depicted the dynamic nature of individual classes of phospholipids, sphingolipids and neutral lipids during mouse preimplantation embryo development.

### Increased lipid unsaturation during mouse and human preimplantation development

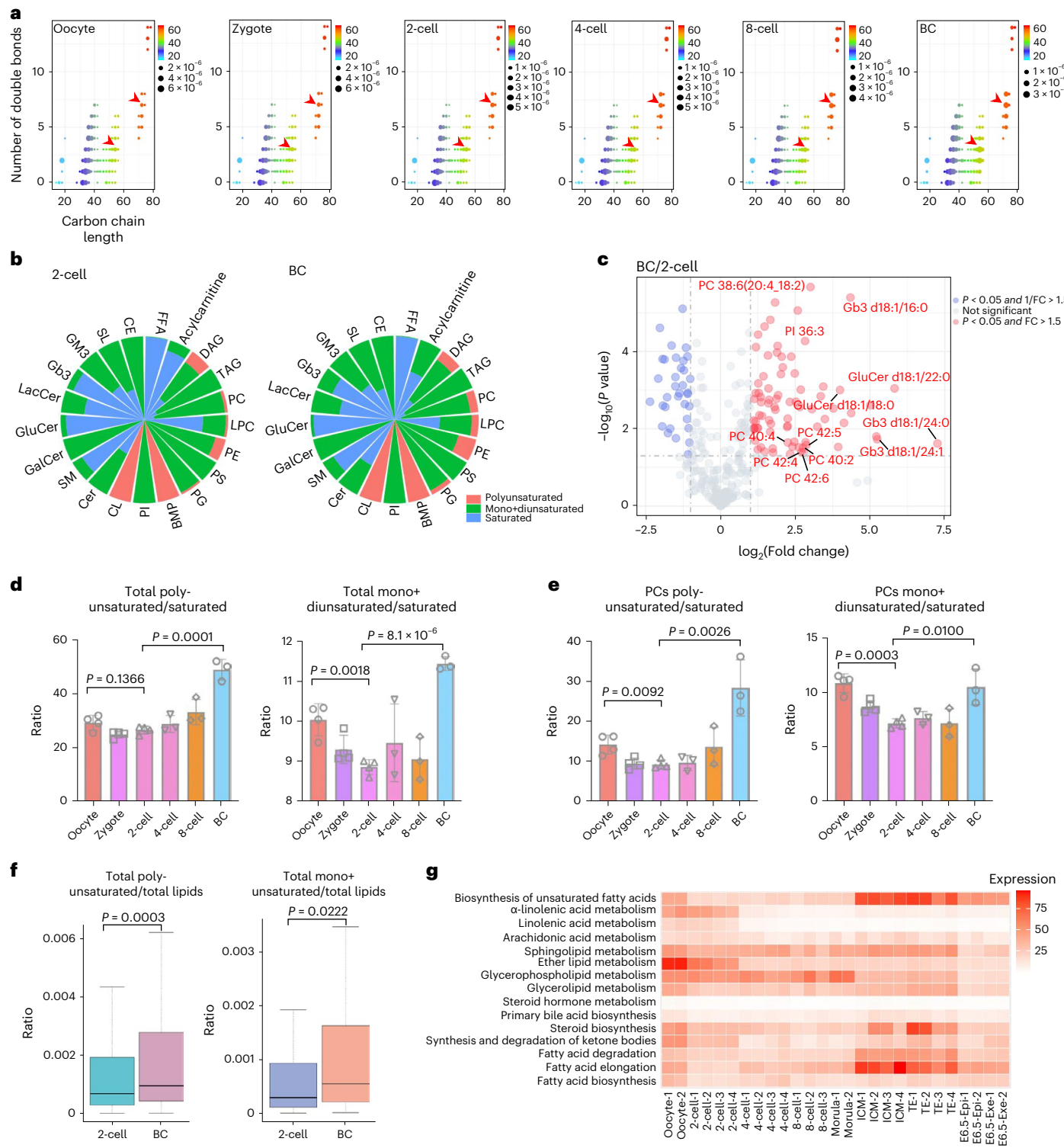
The cell membrane consists of lipid bilayers with phospholipids and assumes a fluid-like feature. This flexible feature facilitates the cellular morphological transformation necessary for sensing the environment by surface receptors, cell division and differentiation<sup>54,55</sup>. The phospholipid composition and the extent of unsaturation have a substantial impact on membrane fluidity<sup>54,56</sup>. The lipidomics profiling results showed that globally, the number of carbon double bonds was increased along with increased hydrocarbon chain length during preimplantation development (Fig. 3a). Thus, all lipids were divided into three categories based on their degree of unsaturation: we designated zero carbon double bonds in the fatty-acid moiety of a lipid species as ‘saturated’; one or two double bonds as ‘monosaturated and diunsaturated’ (mono+diunsaturated); and greater than two double bonds as ‘polyunsaturated’. First, we found that PCs, PEs, CLs and bis(monoacylglycerol)phosphates (BMPs) were more characteristic of the polyunsaturated property than other classes based on the number of polyunsaturated species found in those classes (Extended Data Fig. 5a). Second, based on the relative concentrations, polyunsaturated species of PCs or PEs were more enriched in the blastocyst than the two-cell embryos (Fig. 3b). Volcano plot analysis also confirmed that unsaturated lipids such as PC 38:6, GluCers and ceramide trihexosides (Gb3s) exhibited markedly increased level at the blastocyst stage (Fig. 3c). Consistently, calculating the sum of all three categories of lipids in each developmental stage revealed that the ratio of averaged mono+diunsaturated versus saturated, or polyunsaturated versus saturated lipids showed a bimodal trend: low in two-cell and high in oocyte and blastocyst stages (Fig. 3d). Individual classes, including PCs (Fig. 3e), lyso-PCs (LPCs), PC Os, PSS, GluCers, sulfatides (SLs) and

**Fig. 3 | The degree of lipid unsaturation is increased during mouse preimplantation embryo development.** **a**, Bubble plots showing the change of carbon chain length and the number of carbon double bonds in total lipid profiles across mouse preimplantation embryo development. The bubble size represents the sum of concentration of lipids containing the defined carbon chain length and numbers of carbon double bonds. The red arrows indicate representative lipids showing the indicated trend. **b**, Nightingale rose charts illustrating the distribution of the sum of the concentration for polyunsaturated, mono+diunsaturated and saturated lipid species in two-cell and blastocyst embryos. FFA, free fatty acid. **c**, Volcano plot showing the significantly changed lipid species when comparing blastocysts to two-cell embryos based on the fold change (FC) and *P* values. Data are from four biological replicates of two-cell stage embryos each and three biological replicates of blastocyst stage embryos each. **d**, Bar graphs showing the ratios of concentrations of total polyunsaturated versus total saturated lipids and total mono+diunsaturated versus total saturated lipids in the six developmental stages. **e**, Bar graphs showing the ratios of concentrations of polyunsaturated PCs versus saturated PCs and mono+diunsaturated PCs versus saturated PCs in the six developmental

stages. For **d,e**, each dot represents one biological replicate, and data are from four biological replicates of oocytes, zygote and two-cell stage embryos each and three biological replicates of four-cell, eight-cell and blastocyst stage embryos each and are presented as the mean  $\pm$  s.e.m. Statistical significance was determined by two-tailed unpaired *t*-test. **f**, Box plots showing the distribution of levels for each polyunsaturated lipid species normalized to the sum of the concentration of saturated plus unsaturated lipids, and the distribution of levels for each mono+diunsaturated lipid species normalized to the sum of the concentration of saturated plus unsaturated lipids in two-cell and blastocyst embryos. Data are from four biological replicates of two-cell stage embryos each and three biological replicates of blastocyst stage embryos each. Statistical significance was determined by two-sided, Wilcoxon signed-rank test. Centre line, median; box, 25th and 75th percentiles; whiskers, 1.5  $\times$  interquartile range (IQR). **g**, KEGG pathway analysis of publicly available bulk RNA-seq data with averaged gene expression shows the dynamic changes of lipid metabolism pathways across embryonic development stages. Epiblast (Epi) and extraembryonic ectoderm (Exe) of E6.5 of post-implantation embryos.

SMs (Extended Data Fig. 5b–g), contributed to the enhanced unsaturation feature in the process of the two-cell-to-blastocyst development. Similar results were obtained by plotting individual polyunsaturated or mono+diunsaturated lipid species distribution (Fig. 3f). Finally, transcriptomics analysis of lipid metabolism genes also identified that ICM and TE cells at the blastocyst stage were mostly enriched in ‘biosynthesis of unsaturated fatty acid’ (Fig. 3g). Altogether, these data demonstrate that the degree of unsaturation, particularly for phospholipids, is increased from the two-cell to the blastocyst stage during embryo development.

To explore the extent to which lipid remodelling is conserved between mouse and human, we profiled the lipidome from the human eight-cell embryo stage (a counterpart of mouse two-cell embryos in terms of the totipotent state<sup>57,58</sup>) to the human blastocyst stage (a counterpart of mouse blastocysts in terms of the pluripotent state<sup>59,60</sup>). The lipidomics profile exhibited a similar trend of changes, such as decreased PI and PE levels, increased CL and TAG levels (Fig. 4a and Supplementary Table 3) and increased degree of unsaturation towards the blastocyst stage (Fig. 4b). The individual lipid classes, such as PGs, BMPs, CLs, PC Os and TAGs (Extended Data



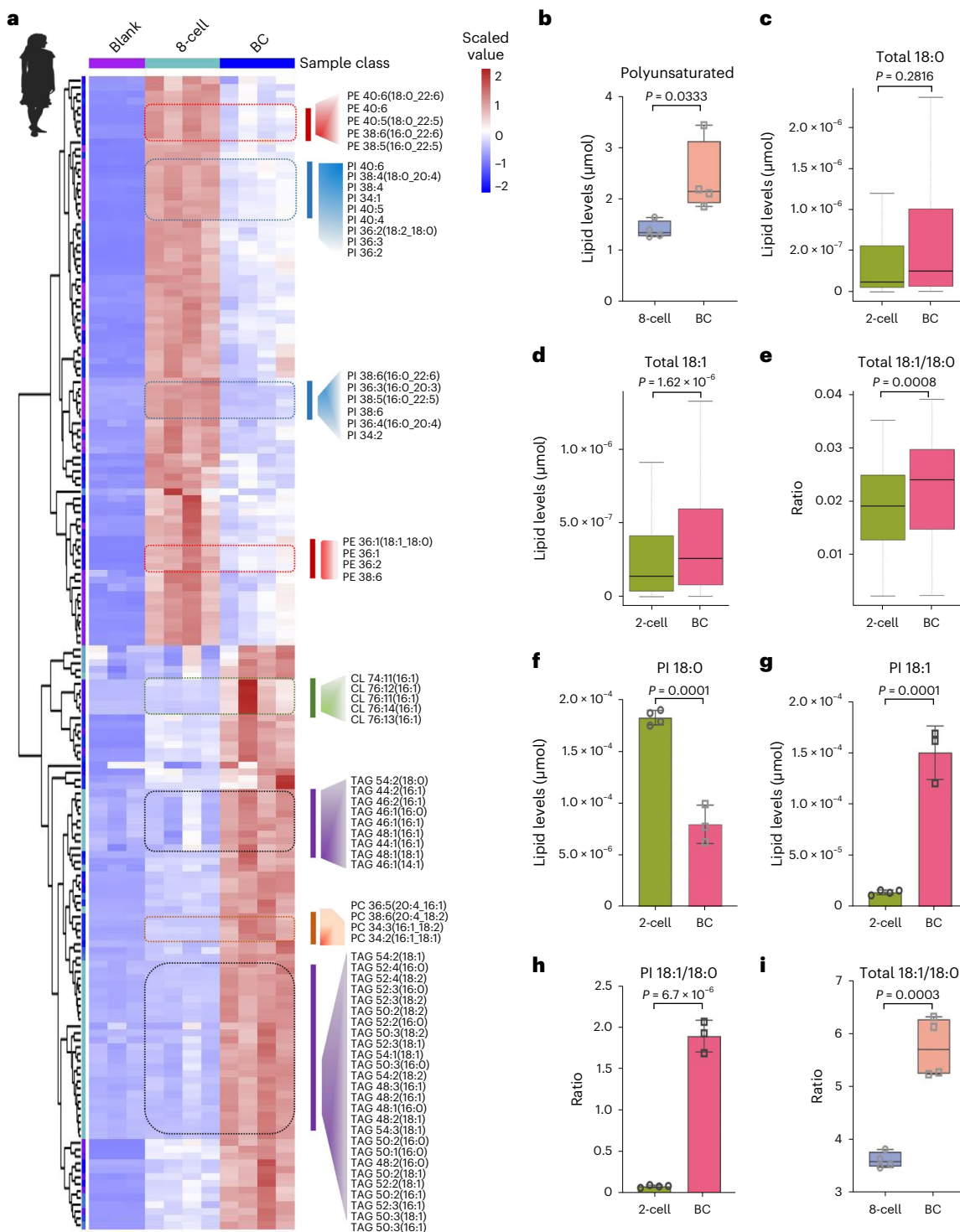


**Fig. 4 | The level of MUFA is increased during mouse and human preimplantation embryo development.** **a**, Heatmap showing the levels of lipids in human eight-cell and blastocyst embryos. Scaled value bar indicates the relative concentration. Data are from four biological replicates of eight-cell and blastocyst stage embryos each. **b**, Box plot showing the sum of the levels of polyunsaturated lipids in total lipids in human eight-cell and blastocyst embryos. Data are from the same biological replicates as in **a**. Statistical significance was determined by two-tailed unpaired *t*-test. **c–e**, Box plots illustrating the levels of stearic acid (C18:0) (**c**), oleic acid (C18:1) (**d**) and the ratio of oleic acid/stearic acid (C18:1/C18:0) (**e**) in total lipids of mouse two-cell

and the blastocyst stage embryos. Statistical significance was determined by two-sided, Wilcoxon signed rank test. **f–h**, Bar graphs showing the levels of C18:0 (**f**), C18:1 (**g**) and C18:1/C18:0 (**h**) in PIs in the mouse two-cell and the blastocyst stage. **i**, Box plot showing the ratio of C18:1/18:0 from human eight-cell and blastocyst embryos. Data are from the same biological replicates as in **a**. Statistical significance was determined by two-tailed unpaired *t*-test. For **c–h**, data are from four biological replicates of two-cell stage embryos each and three biological replicates of blastocyst stage embryos each. Statistical significance was determined by two-tailed unpaired *t*-test. For **b–e,i**, centre line, median; box, 25th and 75th percentiles; whiskers,  $1.5 \times \text{IQR}$ .

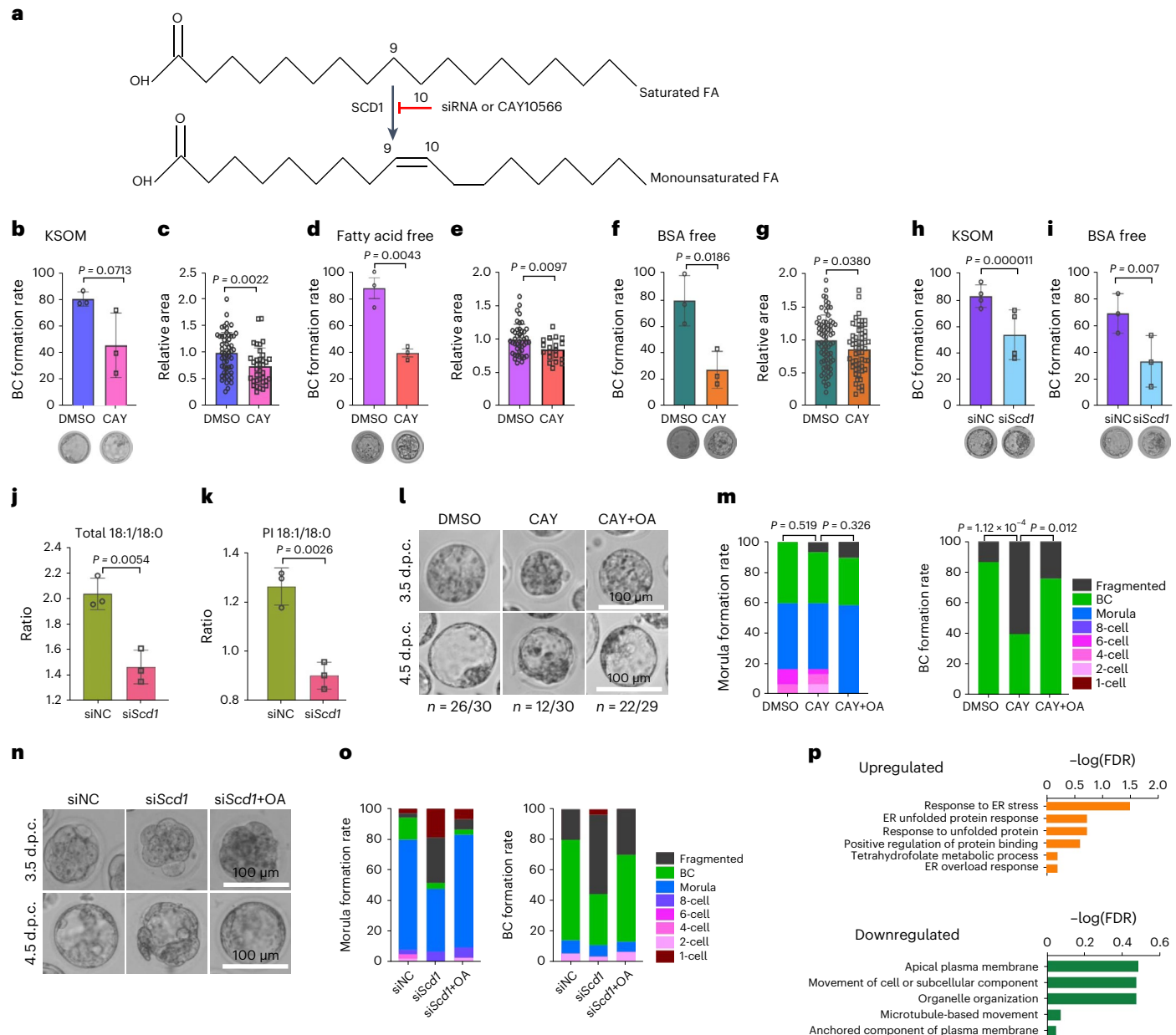


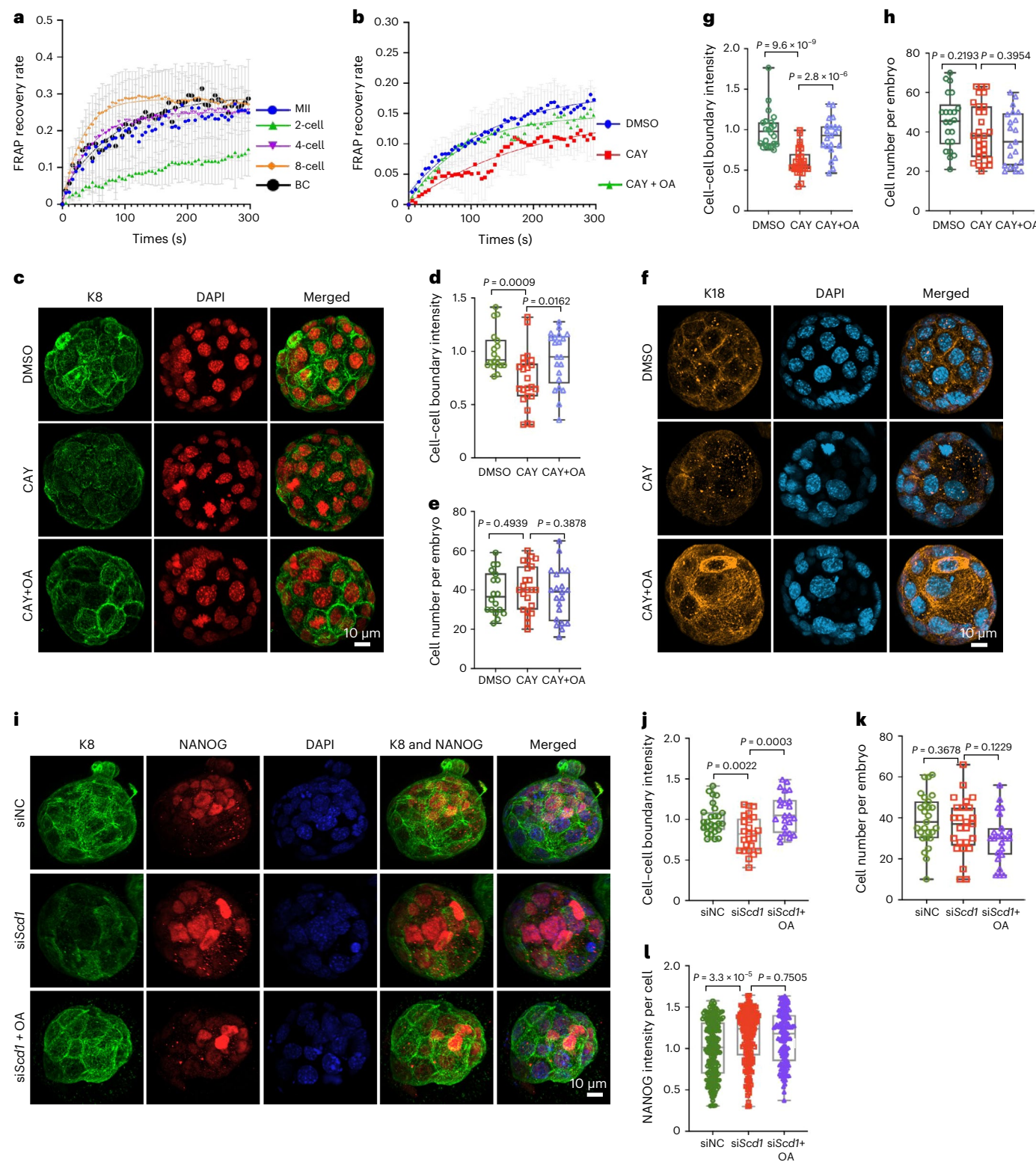
**Fig. 5 | Lipid unsaturation contributes to the developmental process towards blastocyst embryos.** **a**, Schematic showing that SCD1 mediates MUFA synthesis, and the approach to block this process. **b,d,f**, Blastocyst formation rate in embryos treated with dimethylsulfoxide (DMSO) or 100 nM CAY10566 (CAY) cultured in regular KSOM medium (**b**), KSOM with fatty-acid-free medium (**d**) or KSOM with BSA-free medium (**f**). Data are from three independent experiments and are presented as the mean  $\pm$  s.e.m. Statistical significance was determined by two-tailed unpaired *t*-test. **c,e,g**, Blastocyst cavity area after treatment with DMSO or CAY10566 and cultured in regular KSOM medium (**c**), KSOM with fatty-acid-free medium (**e**) or KSOM with BSA-free medium (**g**). Each dot represents one blastocyst. Data for **c**:  $n = 54$  for DMSO and  $n = 36$  for CAY10566-treated blastocysts, the experiments were repeated three times. Data for **e**:  $n = 43$  for DMSO and  $n = 19$  for CAY10566-treated blastocysts, the experiments were repeated three times. Data for **g**:  $n = 74$  for DMSO and  $n = 56$  for CAY10566-treated blastocysts, the experiments were repeated three times. Data are presented as the mean  $\pm$  s.e.m. Statistical significance was determined by two-tailed unpaired

*t*-test. **h,i**, Blastocyst formation rate after knocking down *Scd1* and cultured in regular KSOM (**h**) or BSA-free KSOM medium (**i**). siNC, scramble siRNA. Each dot represents one blastocyst. Data in **h** are from four independent experiments and data in **i** are from three independent experiments. Data are presented as the mean  $\pm$  s.e.m. Statistical significance was determined by chi-squared test. **j,k**, Bar graphs showing the ratio of C18:1/C18:0 of total lipids (**j**) and PIs (**k**) after knocking down *Scd1*. Each dot represents one replicate; data are from three biological replicates and are presented as the mean  $\pm$  s.e.m. Statistical significance was determined by two-tailed unpaired *t*-test. **l,n**, Representative images of mouse embryos at 3.5 or 4.5 d.p.c. that were treated with inhibitor (**l**) or si*Scd1* (**n**). OA, oleic acid. **m,o**, Stacked column graphs showing fractions of embryos at different developmental stages after treated with the inhibitor (**m**) or si*Scd1* (**o**). The data in **m** are presented as the mean  $\pm$  s.e.m. Statistical significance was determined by chi-squared test. **p**, Gene Ontology analysis of upregulated and downregulated genes in *Scd1* knockdown embryos compared with scramble controls. Each condition contains three biological replicates. FDR, false discovery rate.

Fig. 5h–l), each showed an increased degree of polyunsaturation that resembled the trend in the corresponding mouse blastocyst versus two-cell embryo stage. Although the role of lipid unsaturation in oocyte maturation has been reported<sup>61</sup>, enhanced unsaturation

during the totipotent-to-pluripotent development has not been elucidated before.

To examine the source of enriched unsaturated lipids during the blastocyst stage, we analysed the de novo synthesis pathways,



which are mediated by the  $\Delta 5$ ,  $\Delta 6$  and  $\Delta 9$  enzymes. Among these,  $\Delta 9$  (stearoyl-CoA desaturase (SCD)) is responsible for forming monounsaturated fatty acids (MUFA) such as palmitoleic acid (C16:1) and oleic acid (C18:1), whereas  $\Delta 5$  and  $\Delta 6$  enzymes are responsible for generating PUFAs<sup>62</sup>. Transcriptome data showed that *Scd1* and *Scd2* were highly expressed at the blastocyst stage (Extended Data Fig. 5m). We therefore examined total levels of C16:0, C18:0, C16:1 and C18:1 and observed an increase in C18:1 content and the C18:1/C18:0 ratio at the mouse blastocyst stage compared with the two-cell embryo stage (Fig. 4c–e), and

the individual class of PIs showed a similar pattern (Fig. 4f–h). For C16:0 and C16:1, both their content and ratio were not significantly changed (Extended Data Fig. 5o). Notably, the ratio of C18:1/C18:0 (Fig. 4i) and C16:1/C16:0 (Extended Data Fig. 5p) both increased in human embryos. These results suggest that SCD1 has a role in early embryo development and that oleic acid might be the more predominant product in mouse early embryos. Therefore, an inhibitor of SCD1 (CAY10566) was used to determine the function of SCD1 in the development of mouse embryos (Fig. 5a). We treated the embryos with the inhibitor starting

**Fig. 6 | The desaturase SCD1 contributes to membrane fluidity and cytoskeleton organization in eight-cell-to-blastocyst development.** **a**, FRAP analysis showing cell membrane fluidity in oocytes, two-cell, four-cell, eight-cell and blastocyst embryos. Data are from three biological replicates and are presented as the mean  $\pm$  s.e.m. **b**, FRAP analysis showing cell membrane fluidity in 3.5 d.p.c. blastocyst embryos treated with DMSO, CAY10566 or CAY10566 plus oleic acid. Data are from three biological replicates and are presented as the mean  $\pm$  s.e.m. **c,f**, Immunofluorescence of K8 (**c**) and K18 (**f**) staining showing their localization in 4.5 d.p.c. blastocyst embryos treated with DMSO, CAY10566 or CAY10566 plus oleic acid. Images are representative of three independent experiments. **d,e,g,h**, Quantification of the fluorescence intensity of the cell–cell boundary (**d,g**) and cell number per embryo (**e,h**) of 4.5 d.p.c. blastocyst embryos treated with DMSO, CAY10566 or CAY10566 plus oleic acid. Each dot represents

one blastocyst. Data are from three independent experiments and are presented as the mean  $\pm$  s.e.m. Statistical significance was determined by two-tailed unpaired *t*-test. Centre line, median; box, 25th and 75th percentiles; whiskers, 1.5  $\times$  IQR. **i**, Immunofluorescence of K8 and NANOG in 4.5 d.p.c. blastocyst embryos treated with siNC, siScd1 or siScd1 plus oleic acid. Images are representative of three independent experiments. **j–l**, Quantification of the fluorescence intensity of the cell–cell boundary (**j**), cell number per embryo (**k**) and NANOG intensity (**l**) in 4.5 d.p.c. blastocyst embryos treated with siNC, siScd1 or siScd1 plus oleic acid. Each dot represents one blastocyst. Data are from three independent experiments and are presented as the mean  $\pm$  s.e.m. Statistical significance was determined by two-tailed unpaired *t*-test. Centre line, median; box, 25th and 75th percentiles; whiskers, 1.5  $\times$  IQR.

from the zygote stage with a nontoxic concentration (Extended Data Fig. 6a,b). The treated embryos exhibited a mildly impaired blastocyst formation rate (Fig. 5b) and a decreased blastocyst cavity area (Fig. 5c) when cultured in KSOM full medium. Embryos in culture may obtain lipids from the culture medium. Therefore, to avoid this issue, we performed the same experiments with KSOM medium containing fatty-acid-free bovine serum albumin (BSA) and with medium without BSA. Blastocyst formation in these culture media was highly impaired, with evident morphological abnormalities (Fig. 5d,f) and significantly decreased cavity area (Fig. 5e,g). To rule out the possibility of nonspecific effects from the small-molecule inhibitors, we used small interfering RNA (siRNA) to knockdown *Scd1* (*siScd1*) in both BSA-containing and BSA-free conditions (Extended Data Fig. 6c). These experiments confirmed the developmental abnormalities observed in the experiments that used the SCD1 inhibitors (Fig. 5h,i). We also validated that following *Scd1* knockdown, the C18:1/C18:0 ratio was reduced (Fig. 5j and Supplementary Table 4), especially for PIs (Fig. 5k). As elongases are also involved in unsaturated fatty-acid synthesis, we also knocked down the highest expressed elongase (*Elov15*) (Extended Data Fig. 6d). We did not find obvious impairment in development (Extended Data Fig. 6e,f), which is probably due to some redundancy. Next, we examined whether supplementation with oleic acid could rescue the phenotype caused by inhibition of *Scd1*. Indeed, the morphological abnormalities and developmental delay of most blastocysts were rescued by oleic acid supplementation in either CAY10566-treated or siRNA treated embryos (Fig. 5l–o). To better understand how *Scd1* affects blastocyst formation, RNA sequencing (RNA-seq) analysis of *siScd1*-treated embryos that reached the blastocyst stage was performed. The analysis showed upregulation of genes involved in ER stress, a result consistent with the fact that ER stress can be caused by exogenously supplemented saturated fatty acids<sup>33,34</sup>. Genes related to apical plasma membrane and microtubule-based movement were

downregulated (Fig. 5p), which suggested that cytoskeleton organization, a process that is crucial for apical domain formation and polarity establishment, might be impaired during eight-cell-to-blastocyst development<sup>63</sup>.

### Desaturases contribute to membrane fluidity and cytoskeleton organization in eight-cell-to-blastocyst stage embryo development

Next, we investigated how altered lipid unsaturation causes defects in blastocyst stage embryos. Using fluorescence recovery after photobleaching (FRAP) analysis, we found that plasma membrane fluidity reduced after the oocyte stage and recovered from the two-cell to blastocyst stage (Fig. 6a and Extended Data Fig. 7a). Notably, inhibition of *Scd1* led to decreased membrane fluidity, which was rescued by supplementation with oleic acid (Fig. 6b and Extended Data Fig. 7b). This result indicated that the desaturase SCD1 had an impact on membrane fluidity by mediating the lipid unsaturation of MUFA. Increased membrane fluidity of blastocysts supports more flexible membrane shape transformation<sup>54</sup>, including the formation of apical domains on the surface of embryos. It is thought that during early embryo development, cytoskeleton components such as keratin can sense internal and external signals to regulate their organization and promote apical domain formation and maintenance<sup>63–65</sup>. To further assess the function of the lipid desaturase SCD1 on cytoskeleton organization, we performed immunofluorescence of keratin 8 (K8) and keratin 18 (K18)<sup>63,66</sup>. We observed that K8 and K18 formed a dense network demarcating the apical domain in the control 3.5 or 4.5 days post coitum (d.p.c.) blastocysts (Fig. 6c,f,i and Extended Data Fig. 8a,e). By contrast, inhibition of *Scd1* by CAY10566 disrupted the organized localization of K8 and K18, shifting their distribution to a more uniform pattern on the embryo surface, and caused an obscured interface at the cell–cell boundary (Fig. 6c,d,f,g and Extended

**Fig. 7 | The desaturases for PUFA synthesis contribute to blastocyst formation by mediating cytoskeleton organization and apical domain formation.** **a**, PUFA including arachidonic acid (ARA), eicosapentaenoic acid (EPA) and docosahexaenoic acid (DHA) are synthesized by desaturases Δ6 and Δ5, which can be inhibited by the indicated inhibitors. **b**, Representative images of mouse embryos at 4.5 d.p.c. treated with DMSO or 100 nM of the Δ6 enzyme inhibitor SC-26196 from zygotes cultured in BSA-free KSOM medium. Images are representative of four independent experiments. **c**, Blastocyst formation rate and cavity area of blastocyst embryos treated with DMSO or SC-26196 grown in BSA-free KSOM medium. Each dot represents one blastocyst, and data of blastocyst formation rate are from four independent experiments. Data of relative area are from  $n = 89$  for DMSO and  $n = 52$  for SC-26196-treated blastocysts, and the experiments were repeated for four times. Data are presented as the mean  $\pm$  s.e.m. Statistical significance was determined by two-tailed unpaired *t*-test. **d**, Representative images of mouse embryos at 4.5 d.p.c. that were treated with DMSO or 100 nM of the Δ5 enzyme inhibitor sesamin cultured in BSA-free KSOM medium. Images shown are representative of three independent experiments. **e**, Blastocyst formation rate and cavity

area of blastocyst embryos treated with DMSO or sesamin grown in BSA-free KSOM medium. Each dot represents one blastocyst, and data of blastocyst formation rate are from three independent experiments. Data of relative area are from  $n = 35$  for DMSO and  $n = 22$  for sesamin-treated blastocysts, and the experiments were repeated for two times. Data are presented as the mean  $\pm$  s.e.m. Statistical significance was determined by two-tailed unpaired *t*-test. **f**, Immunofluorescence of K18 and CDX2 in 4.5 d.p.c. blastocyst embryos treated with DMSO, sesamin, sesamin plus ARA or sesamin plus EPA. **g–i**, Quantification of the fluorescence intensity of the cell–cell boundary (**g**), cell number per embryo (**h**) and CDX2 intensity (**i**) in 4.5 d.p.c. blastocyst embryos treated with DMSO, sesamin, sesamin plus ARA or sesamin plus EPA. For **f–i**, data are from  $n = 21$  for DMSO,  $n = 28$  for sesamin,  $n = 17$  for sesamin + ARA and  $n = 16$  for sesamin + EPA. The experiments were repeated three times (for DMSO and sesamin) and two times (for sesamin + ARA and sesamin + EPA). Data are presented as the mean  $\pm$  s.e.m. Statistical significance was determined by two-tailed unpaired *t*-test. Centre line, median; box, 25th and 75th percentiles; whiskers, 1.5  $\times$  IQR.

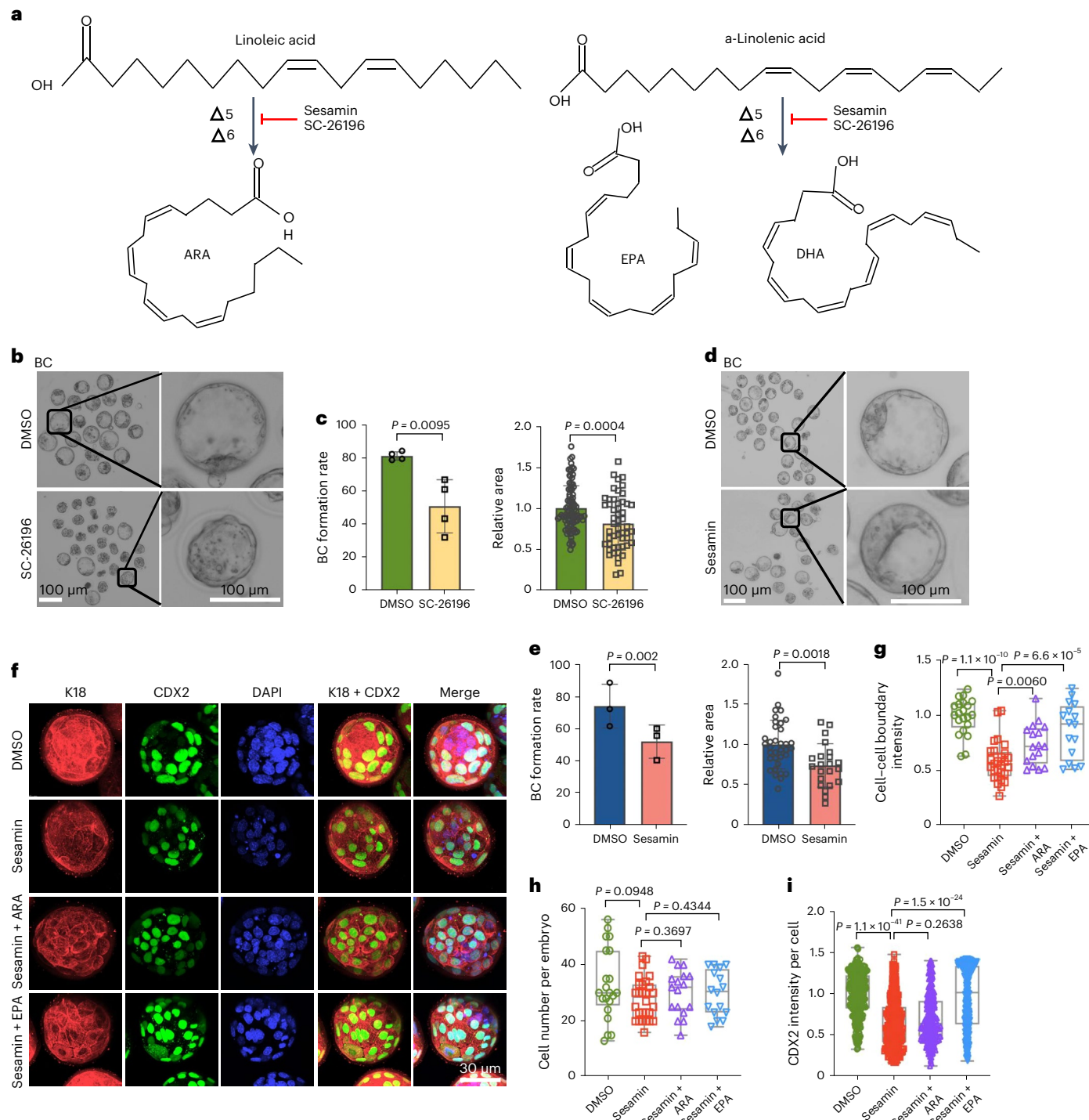
Data Fig. 8a,b), without largely influencing the cell number (Fig. 6e,h) and Extended Data Fig. 8c,d). These results were further consolidated by knocking down *Scd1* (Fig. 6i–l and Extended Data Fig. 8e–g). Notably, this effect could be rescued by supplementation with oleic acid (Fig. 6c,d,f,g,i,j and Extended Data Fig. 8a,b,e,f), which demonstrates that this lipid desaturase contributes to proper cytoskeleton organization in blastocyst development.

Mammalian cells can synthesize PUFAs through desaturases such as Δ6 and Δ5 (encoded by *Fads1/2*) (Fig. 7a and Extended Data Fig. 5n). Based on our findings that polyunsaturation also increased at the blastocyst stage (Fig. 3 and Extended Data Fig. 5), we wondered whether desaturases Δ6 and Δ5 had the same contribution to embryo development as SCD1. Indeed, inhibition of Δ6 or Δ5 with SC-26196 or sesamin markedly impaired blastocyst formation and reduced the cavity area

(Fig. 7b–e). Similarly, treatment with either inhibitor caused disrupted cytoskeleton organization and blurry cell–cell boundary (Fig. 7f–i), which can be rescued by supplementation of PUFAs eicosapentaenoic acid (EPA) (Fig. 7f–i). Taken together, our data demonstrate that the desaturases for both MUFA and PUFA synthesis are essential for early embryo development by contributing to cytoskeleton organization which is required for apical domain formation.

### Desaturases contribute to the establishment of apical–basal polarity of early embryos for successful implantation of blastocysts in the uterus

Mouse early embryo development from the eight-cell to blastocyst stage requires apical and basolateral domain formation to establish apical–basal polarity, facilitate blastocyst formation and support



blastocyst implantation in the uterus<sup>64</sup>. We therefore asked whether SCD1 is required for these vital steps during early development. The apical protein ezrin connects the plasma membrane and cytoskeleton, and its phosphorylation at T567 is required for binding the cytoskeleton protein F-actin<sup>67</sup>. Treatment with CAY10566 led to reduced phosphorylated ezrin enrichment at the apical domain in eight-cell embryos (Fig. 8a,b) and disrupted the pattern of phosphorylated ezrin in blastocysts (Fig. 8e,f). Another polarity protein,  $\alpha$ PKC, did not exhibit changes in levels in eight-cell embryos, but was mildly decreased in blastocysts (Fig. 8a,c,e,g). Moreover, the expression of the basolateral protein E-cadherin was decreased when SCD1 was inhibited in eight-cell and blastocyst embryos (Fig. 8a,d,e,h). As our previous analysis showed that inhibition of SCD1 led to decreased membrane fluidity (Fig. 6b), a closer examination revealed that the fluidity of ezrin and F-actin, the lateral mobility of which is required for polarity establishment<sup>68</sup>, was attenuated when treated with CAY10566 (Fig. 8j,k). This effect was rescued through supplementation with oleic acid (Fig. 8j,k). Together, these data demonstrate that SCD1 is required for establishment of apical–basal polarity to support eight-cell-to-blastocyst development by regulating the fluidity of polarity and cytoskeleton proteins. As apical–basal polarity promotes TE cell specification<sup>69</sup>, we also found that nuclear expression of the TE transcription factor YAP was reduced in SCD1-inhibited blastocysts (Fig. 8e,i). Moreover, when we transferred blastocysts to the uterus of pseudo-pregnant recipient mice (Fig. 8l), the SCD1-inhibited blastocysts formed significantly less deciduae compared with the controls (Fig. 8m,n and Extended Data Fig. 9a). Expression of the extraembryonic marker K18 in embryonic day 7.5 (E7.5) embryos was also reduced (Fig. 8o). In summary, these results demonstrate that SCD1 regulates the molecular events in apical–basal polarity establishment during eight-cell-to-blastocyst development to support the physiological function of blastocyst implantation in the uterus.

#### Desaturases contribute to blastoid generation from mouse ESCs

Finally, as the mouse blastocyst is composed of ICM and TE cell lineages, we examined their in vitro cultured counterparts, mouse embryonic stem cells (ESCs) and trophoblast stem cells (TSCs), respectively, to see whether apical–basal epithelial polarity and cytoskeleton were influenced by lipid unsaturation. The results revealed that the basolateral protein E-cadherin showed reduced expression in both ESCs and TSCs after treatment with CAY10566, SC-26196 or sesamin, and the cells became disconnected and blurry at the demarcating cell–cell boundary, especially in cells treated with SC-26196 or sesamin (Extended Data

Fig. 9b,c). The cytoskeleton proteins K8 and K18 were also decreased and became disorganized after treatment in TSCs (Extended Data Fig. 9d,e). Moreover, the apical protein ezrin showed slightly lower T567 phosphorylation after treatment in ESCs and TSCs (Extended Data Fig. 9f,g). These results demonstrate that lipid unsaturation affects apical–basal polarity in cultured embryonic cells.

Given the high similarity between the processes of blastoid generation and blastocyst formation<sup>70</sup>, we asked whether increased lipid unsaturation is required during blastoid establishment. We inhibited desaturase activity in the induction medium for blastoid generation from extended/expended potential stem cells<sup>70</sup> (Fig. 8p and Extended Data Fig. 10a), and the efficiency was reduced compared with the control cells (Fig. 8q,r and Extended Data Fig. 10b,c). Recapitulating the results from blastocyst embryos, we found decreased expression of E-cadherin and K18 in blastoids after treatment with CAY10566, SC-26196 or sesamin (Fig. 8s and Extended Data Fig. 10d). Taken together, these data demonstrate that increased lipid unsaturation is important for embryonic cell polarization and blastoid generation.

#### Discussion

Fertilized zygotes require proper nutrients for metabolism and successful development. How intracellular metabolites and metabolic pathways are remodelled during this process is a longstanding unanswered question owing to the scarcity of materials. Evolving MS technologies have enabled us to profile cellular metabolomes and lipidomes<sup>10,15,22,71</sup>. Using MS-based ultrasensitive targeted metabolomics and lipidomics of a small number of embryos, we comprehensively investigated the lipidomic remodelling process of different categories of lipids from the oocyte to blastocyst embryo stage. Our data delineated a dynamic lipid landscape of mammalian preimplantation embryo development. Each stage has its distinct lipidomics signature, which indicates that the physiological requirements of lipids for different developmental stages vary greatly. Of note, the lipid extraction methods we used here are the IPA extraction method, which recovers polar lipids such as phospholipids with good efficiency<sup>72</sup>, and the Bligh&Dyer extraction method, which recovers both polar phospholipids and neutral lipids. Changes in phospholipid levels were cross-validated using these two different methods, and phospholipids represented the major cellular membrane lipid constituents and influenced membrane fluidity and apical–basal polarity establishment.

Our lipidomics analysis unravelled a higher degree of unsaturation in the oocyte and blastocyst stages than in the two-cell embryo stage. The degree of unsaturation in oocytes echoes a previous observation that a high content of PUFAs is essential for oocyte meiosis and

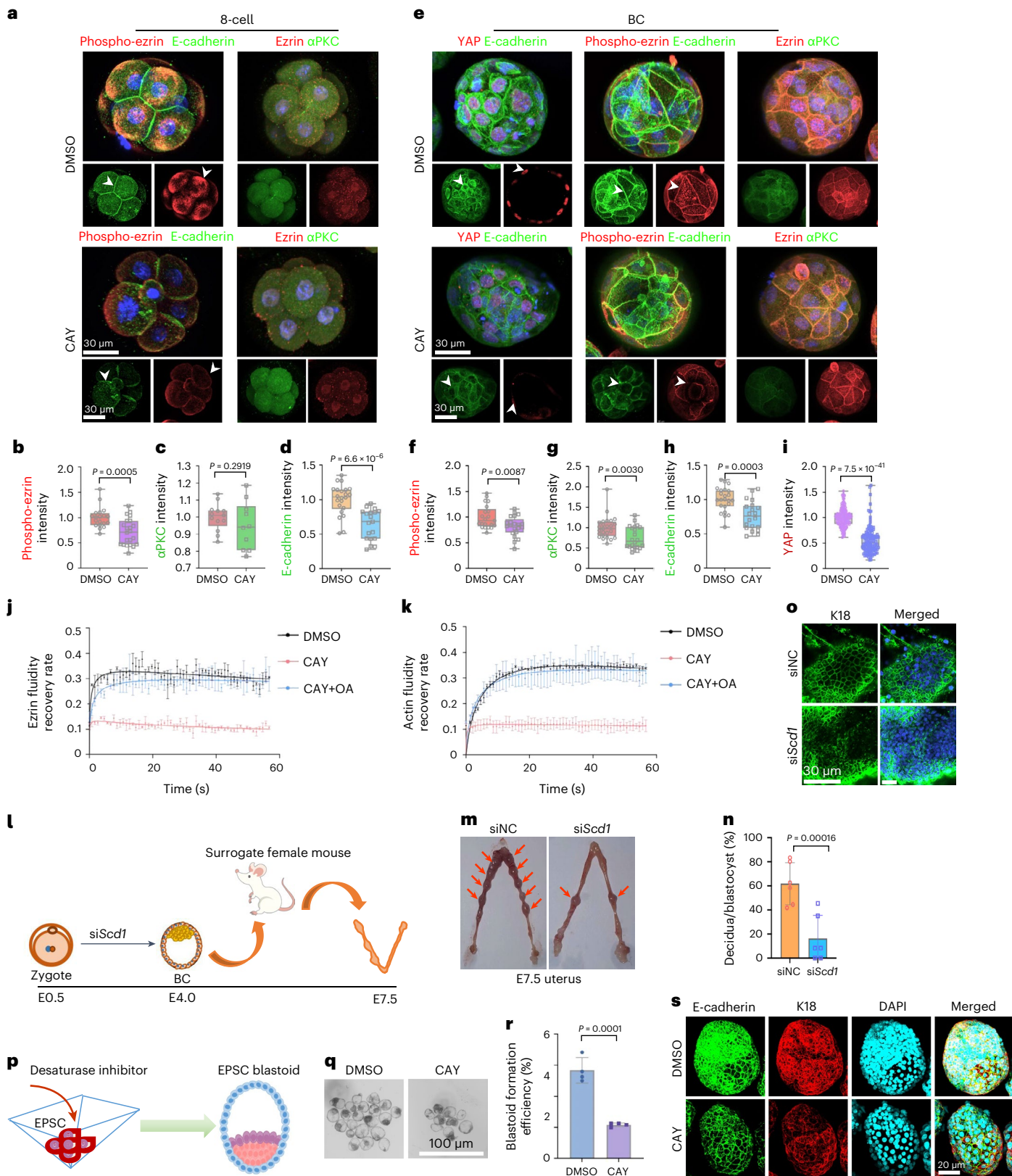
**Fig. 8 | Desaturases contribute to the establishment of apical–basal polarity of early embryos for successful implantation of blastocysts in the uterus.**

**a**, Immunofluorescence of phosphorylated ezrin (phospho-ezrin), E-cadherin, ezrin and  $\alpha$ PKC staining showing their localization in eight-cell stage embryos treated with DMSO or CAY10566. The arrowheads indicate the location of phospho-ezrin and E-cadherin. **b–d**, Quantification of the fluorescence intensity of phospho-ezrin (**b**),  $\alpha$ PKC (**c**) and E-cadherin (**d**). Each dot represents one blastocyst. Data in **b**, **d** are from three independent experiments. Data in **c**:  $n = 13$  for DMSO and  $n = 10$  for CAY10566-treated blastocysts. The experiments were repeated two times. Data are presented as the mean  $\pm$  s.e.m. Statistical significance was determined by two-tailed unpaired *t*-test. Centre line, median; box, 25th and 75th percentiles; whiskers,  $1.5 \times$  IQR. **e**, Immunofluorescence of E-cadherin, ezrin,  $\alpha$ PKC, phospho-ezrin and YAP staining showing their localization in blastocyst stage embryos treated with DMSO or CAY10566. Images are representative of three independent experiments. The arrowheads indicate the location of YAP, phospho-ezrin and E-cadherin. **f–i**, Quantification of the fluorescence intensity of phospho-ezrin (**f**),  $\alpha$ PKC (**g**), E-cadherin (**h**) and YAP (**i**). Each dot represents one blastocyst. Data are from three independent experiments and are presented as the mean  $\pm$  s.e.m. Statistical significance was determined by two-tailed unpaired *t*-test. Centre line, median; box, 25th and 75th percentiles; whiskers;  $1.5 \times$  IQR. **j,k**, FRAP analysis showing the fluidity of ezrin (**j**)

and F-actin (**k**) in eight-cell embryos treated with DMSO or CAY10566. Data are from three biological replicates and are presented as the mean  $\pm$  s.e.m. **l**, Timeline of the embryo transfer experiment. **m**, E7.5 deciduae induced by transferred blastocysts. Arrows indicate formed deciduae. **n**, Quantification of decidua formation efficiency. Each dot represents an independent embryo transfer experiment. Data are from six biological experiments and are presented as the mean  $\pm$  s.e.m. Statistical significance was determined by two-tailed unpaired *t*-test. **o**, Immunofluorescence of K18 localization at E7.5 conceptus. Images are representative of three biological replicates. **p**, Diagram showing the process of extended/expended potential stem cell (EPSC)-induced blastoid formation with desaturase inhibitors. **q**, Phase-contrast images of EPSC blastoids treated with DMSO or CAY10566. **r**, Quantification of blastoid formation efficiency in EPSC blastoids treated with DMSO or CAY10566. Data are presented as the mean  $\pm$  s.e.m. Statistical significance was determined by two-tailed unpaired *t*-test. **s**, Immunofluorescence of E-cadherin and K18 localization in EPSC blastoids treated with DMSO or CAY10566. For **q–s**, data are from four independent experiments. The larger pictures are three-dimensional reconstituted ones and the smaller pictures are two-dimensional slice ones, which are from the same embryos except for the phospho-ezrin and E-cadherin staining images for cells treated with CAY10566.

maturity<sup>61</sup>. The surprising finding here is that the transition towards more unsaturated lipid profiles during late preimplantation embryogenesis contributes to increased cell membrane fluidity. The enhanced fluidity can affect membrane shape formation, such as generating the apical and basolateral domains required during eight-cell-to-blastocyst development<sup>54</sup>. It can also influence the distribution of cytoskeleton

proteins, which are associated with the apical and basolateral domains in the membrane and integrate environmental signals to further influence cell morphology and cell fate determination<sup>64,66</sup>. With further pharmacological and genetic approaches, we identified a pivotal role of the desaturase SCD1 in this process through its function in producing MUFA, and lipid unsaturation mediates blastocyst formation and



successful implantation. Unlike previous studies that supplemented exogenous saturated or unsaturated fatty acids to embryos, we elucidated the mechanisms of how endogenous lipid unsaturation and the metabolic enzymes involved can regulate the developmental process (Extended Data Fig. 10e). Even though *Scd1* knockout mice are not embryonic lethal, *SCD1* inhibition in a defined medium condition is detrimental to embryonic cells and embryo development<sup>73</sup>. This difference is perhaps because *in vivo*, embryos can take up fatty acids from the environment of the reproductive tract to compensate for a loss of desaturases.

Taken together, our study provides a comprehensive lipidomics profile of mammalian early embryo development. The massive lipid remodelling of many species calls for further investigation for each of the regulatory mechanisms as well as downstream physiological impact, beyond our current focus on lipid unsaturation. In the future, the lipidomic fingerprints with distinct features discovered here, especially those measurable by noninvasive instruments such as Raman spectrometers<sup>24,25</sup>, can provide opportunities for assessing embryo quality and developmental potential to improve the success rate of *in vitro* fertilization procedures.

## Online content

Any methods, additional references, Nature Portfolio reporting summaries, source data, extended data, supplementary information, acknowledgements, peer review information; details of author contributions and competing interests; and statements of data and code availability are available at <https://doi.org/10.1038/s41556-023-01341-3>.

## References

1. Rossant, J. Genetic control of early cell lineages in the mammalian embryo. *Annu. Rev. Genet.* **52**, 185–201 (2018).
2. Li, L., Zheng, P. & Dean, J. Maternal control of early mouse development. *Development* **137**, 859–870 (2010).
3. Wu, J. et al. The landscape of accessible chromatin in mammalian preimplantation embryos. *Nature* **534**, 652–657 (2016).
4. Wang, C. et al. Reprogramming of H3K9me3-dependent heterochromatin during mammalian embryo development. *Nat. Cell Biol.* **20**, 620–631 (2018).
5. Xue, Z. et al. Genetic programs in human and mouse early embryos revealed by single-cell RNA sequencing. *Nature* **500**, 593–597 (2013).
6. Gao, Y. et al. Protein expression landscape of mouse embryos during pre-implantation development. *Cell Rep.* **21**, 3957–3969 (2017).
7. Zhang, J. et al. Metabolism in pluripotent stem cells and early mammalian development. *Cell Metab.* **27**, 332–338 (2018).
8. Chi, F., Sharpley, M. S., Nagaraj, R., Roy, S. S. & Banerjee, U. Glycolysis-independent glucose metabolism distinguishes TE from ICM fate during mammalian embryogenesis. *Dev. Cell* **53**, 9–26.e24 (2020).
9. Nagaraj, R. et al. Nuclear localization of mitochondrial TCA cycle enzymes as a critical step in mammalian zygotic genome activation. *Cell* **168**, 210–223.e211 (2017).
10. Zhao, J. et al. Metabolic remodelling during early mouse embryo development. *Nat. Metab.* **3**, 1372–1384 (2021).
11. van Meer, G., Voelker, D. R. & Feigenson, G. W. Membrane lipids: where they are and how they behave. *Nat. Rev. Mol. Cell Biol.* **9**, 112–124 (2008).
12. Li, J. et al. Lipid desaturation is a metabolic marker and therapeutic target of ovarian cancer stem cells. *Cell Stem Cell* **20**, 303–314.e305 (2017).
13. Simons, K. & Toomre, D. Lipid rafts and signal transduction. *Nat. Rev. Mol. Cell Biol.* **1**, 31–39 (2000).
14. Guan, X. L. et al. Biochemical membrane lipidomics during *Drosophila* development. *Dev. Cell* **24**, 98–111 (2013).
15. Fraher, D. et al. Zebrafish embryonic lipidomic analysis reveals that the yolk cell is metabolically active in processing lipid. *Cell Rep.* **14**, 1317–1329 (2016).
16. Dunning, K. R. et al. Beta-oxidation is essential for mouse oocyte developmental competence and early embryo development. *Biol. Reprod.* **83**, 909–918 (2010).
17. Dunning, K. R., Akison, L. K., Russell, D. L., Norman, R. J. & Robker, R. L. Increased beta-oxidation and improved oocyte developmental competence in response to l-carnitine during ovarian *in vitro* follicle development in mice. *Biol. Reprod.* **85**, 548–555 (2011).
18. Ferguson, E. M. & Leese, H. J. Triglyceride content of bovine oocytes and early embryos. *J. Reprod. Fertil.* **116**, 373–378 (1999).
19. Ferguson, E. M. & Leese, H. J. A potential role for triglyceride as an energy source during bovine oocyte maturation and early embryo development. *Mol. Reprod. Dev.* **73**, 1195–1201 (2006).
20. Sturmey, R. G. & Leese, H. J. Energy metabolism in pig oocytes and early embryos. *Reproduction* **126**, 197–204 (2003).
21. Sturmey, R. G., Reis, A., Leese, H. J. & McEvoy, T. G. Role of fatty acids in energy provision during oocyte maturation and early embryo development. *Reprod. Domest. Anim.* **44**, 50–58 (2009).
22. Sudano, M. J. et al. Lipidome signatures in early bovine embryo development. *Theriogenology* **86**, 472–484.e471 (2016).
23. Watanabe, T. et al. Characterisation of the dynamic behaviour of lipid droplets in the early mouse embryo using adaptive harmonic generation microscopy. *BMC Cell Biol.* **11**, 38 (2010).
24. Bradley, J. et al. Quantitative imaging of lipids in live mouse oocytes and early embryos using CARS microscopy. *Development* **143**, 2238–2247 (2016).
25. Hu, F., Shi, L. & Min, W. Biological imaging of chemical bonds by stimulated Raman scattering microscopy. *Nat. Methods* **16**, 830–842 (2019).
26. Tatsumi, T. et al. Forced lipophagy reveals that lipid droplets are required for early embryonic development in mouse. *Development* **145**, dev161893 (2018).
27. Aizawa, R. et al. Synthesis and maintenance of lipid droplets are essential for mouse preimplantation embryonic development. *Development* **146**, dev181925 (2019).
28. Al Darwich, A. et al. Effect of PUFA on embryo cryoresistance, gene expression and AMPKα phosphorylation in IVF-derived bovine embryos. *Prostaglandins Other Lipid Mediat.* **93**, 30–36 (2010).
29. McKeegan, P. J. & Sturmey, R. G. The role of fatty acids in oocyte and early embryo development. *Reprod. Fertil. Dev.* **24**, 59–67 (2011).
30. Van Hoeck, V. et al. Oocyte developmental failure in response to elevated nonesterified fatty acid concentrations: mechanistic insights. *Reproduction* **145**, 33–44 (2013).
31. Fayezi, S., Leroy, J., Ghaffari Novin, M. & Darabi, M. Oleic acid in the modulation of oocyte and preimplantation embryo development. *Zygote* **26**, 1–13 (2018).
32. Calder, M. D. et al. Effects of palmitic acid on localization of embryo cell fate and blastocyst formation gene products. *Reproduction* **163**, 133–143 (2022).
33. Wu, L. L., Russell, D. L., Norman, R. J. & Robker, R. L. Endoplasmic reticulum (ER) stress in cumulus-oocyte complexes impairs pentraxin-3 secretion, mitochondrial membrane potential ( $\Delta\Psi_m$ ), and embryo development. *Mol. Endocrinol.* **26**, 562–573 (2012).
34. Sutton-McDowall, M. L. et al. Nonesterified fatty acid-induced endoplasmic reticulum stress in cattle cumulus oocyte complexes alters cell metabolism and developmental competence. *Biol. Reprod.* **94**, 23 (2016).
35. Wonnacott, K. E. et al. Dietary omega-3 and -6 polyunsaturated fatty acids affect the composition and development of sheep granulosa cells, oocytes and embryos. *Reproduction* **139**, 57–69 (2010).

36. Yousif, M. D. et al. Oleic acid counters impaired blastocyst development induced by palmitic acid during mouse preimplantation development: understanding obesity-related declines in fertility. *Reprod. Sci.* **27**, 2038–2051 (2020).
37. Leung, Z. C. L., Abu Rafea, B., Watson, A. J. & Betts, D. H. Free fatty acid treatment of mouse preimplantation embryos demonstrates contrasting effects of palmitic acid and oleic acid on autophagy. *Am. J. Physiol. Cell Physiol.* **322**, C833–C848 (2022).
38. Fahy, E. et al. Update of the LIPID MAPS comprehensive classification system for lipids. *J. Lipid Res.* **50**, S9–S14 (2009).
39. Conesa, A., Nueda, M. J., Ferrer, A. & Talón, M. maSigPro: a method to identify significantly differential expression profiles in time-course microarray experiments. *Bioinformatics* **22**, 1096–1102 (2006).
40. Shannon, C. E. A mathematical theory of communication. *Bell Syst. Tech. J.* **27**, 379–423 (1948).
41. Höring, M. et al. Benchmarking one-phase lipid extractions for plasma lipidomics. *Anal. Chem.* **94**, 12292–12296 (2022).
42. Braverman, N. E. & Moser, A. B. Functions of plasmalogen lipids in health and disease. *Biochim. Biophys. Acta* **1822**, 1442–1452 (2012).
43. Honsho, M. & Fujiki, Y. Plasmalogen homeostasis—regulation of plasmalogen biosynthesis and its physiological consequence in mammals. *FEBS Lett.* **591**, 2720–2729 (2017).
44. Mankidy, R. et al. Membrane plasmalogen composition and cellular cholesterol regulation: a structure activity study. *Lipids Health Dis.* **9**, 62 (2010).
45. Almsherqi, Z. A. Potential role of plasmalogens in the modulation of biomembrane morphology. *Front. Cell Dev. Biol.* **9**, 673917 (2021).
46. Zoeller, R. A. et al. Plasmalogens as endogenous antioxidants: somatic cell mutants reveal the importance of the vinyl ether. *Biochem. J.* **338**, 769–776 (1999).
47. Hammond, G. R. V. & Burke, J. E. Novel roles of phosphoinositides in signaling, lipid transport, and disease. *Curr. Opin. Cell Biol.* **63**, 57–67 (2020).
48. Machaty, Z. Signal transduction in mammalian oocytes during fertilization. *Cell Tissue Res.* **363**, 169–183 (2016).
49. Ye, C., Shen, Z. & Greenberg, M. L. Cardiolipin remodeling: a regulatory hub for modulating cardiolipin metabolism and function. *J. Bioenerg. Biomembr.* **48**, 113–123 (2016).
50. Luévanos-Martínez, L. A. & Kowaltowski, A. J. Phosphatidylglycerol-derived phospholipids have a universal, domain-crossing role in stress responses. *Arch. Biochem. Biophys.* **585**, 90–97 (2015).
51. Hannun, Y. A. & Obeid, L. M. Principles of bioactive lipid signalling: lessons from sphingolipids. *Nat. Rev. Mol. Cell Biol.* **9**, 139–150 (2008).
52. Lam, S. M. et al. A multi-omics investigation of the composition and function of extracellular vesicles along the temporal trajectory of COVID-19. *Nat. Metab.* **3**, 909–922 (2021).
53. Arena, R. et al. Lipid droplets in mammalian eggs are utilized during embryonic diapause. *Proc. Natl Acad. Sci. USA* **118**, e2018362118 (2021).
54. Lipowsky, R. Remodeling of membrane compartments: some consequences of membrane fluidity. *Biol. Chem.* **395**, 253–274 (2014).
55. Dawaliby, R. et al. Phosphatidylethanolamine is a key regulator of membrane fluidity in eukaryotic cells. *J. Biol. Chem.* **291**, 3658–3667 (2016).
56. Wiktorowska-Owczarek, A., Berezińska, M. & Nowak, J. Z. PUFAs: structures, metabolism and functions. *Adv. Clin. Exp. Med.* **24**, 931–941 (2015).
57. Aoki, F., Worrad, D. M. & Schultz, R. M. Regulation of transcriptional activity during the first and second cell cycles in the preimplantation mouse embryo. *Dev. Biol.* **181**, 296–307 (1997).
58. Braude, P., Bolton, V. & Moore, S. Human gene expression first occurs between the four- and eight-cell stages of preimplantation development. *Nature* **332**, 459–461 (1988).
59. Mazid, M. A. et al. Rolling back human pluripotent stem cells to an eight-cell embryo-like stage. *Nature* **605**, 315–324 (2022).
60. Sharpley, M. S., Chi, F., Hoeve, J. T. & Banerjee, U. Metabolic plasticity drives development during mammalian embryogenesis. *Dev. Cell* **56**, 2329–2347.e6 (2021).
61. Li, L. et al. Characterization of metabolic patterns in mouse oocytes during meiotic maturation. *Mol. Cell* **80**, 525–540.e9 (2020).
62. Nakamura, M. T. & Nara, T. Y. Structure, function, and dietary regulation of Δ6, Δ5, and Δ9 desaturases. *Annu. Rev. Nutr.* **24**, 345–376 (2004).
63. Lim, H. Y. G. et al. Keratins are asymmetrically inherited fate determinants in the mammalian embryo. *Nature* **585**, 404–409 (2020).
64. Lim, H. Y. G. & Plachta, N. Cytoskeletal control of early mammalian development. *Nat. Rev. Mol. Cell Biol.* **22**, 548–562 (2021).
65. Lu, H., Hesse, M., Peters, B. & Magin, T. M. Type II keratins precede type I keratins during early embryonic development. *Eur. J. Cell Biol.* **84**, 709–718 (2005).
66. Coulombe, P. A. & Wong, P. Cytoplasmic intermediate filaments revealed as dynamic and multipurpose scaffolds. *Nat. Cell Biol.* **6**, 699–706 (2004).
67. Liu, H. et al. Atypical PKC, regulated by Rho GTPases and Mek/Erk, phosphorylates ezrin during eight-cell embryocompaction. *Dev. Biol.* **375**, 13–22 (2013).
68. Zhu, M. et al. Developmental clock and mechanism of de novo polarization of the mouse embryo. *Science* **370**, eabd2703 (2020).
69. Zhu, M. & Zernicka-Goetz, M. Principles of self-organization of the mammalian embryo. *Cell* **183**, 1467–1478 (2020).
70. Li, R. et al. Generation of blastocyst-like structures from mouse embryonic and adult cell cultures. *Cell* **179**, 687–702.e18 (2019).
71. Ferreira, C. R., Pirro, V., Eberlin, L. S., Hallett, J. E. & Cooks, R. G. Developmental phases of individual mouse preimplantation embryos characterized by lipid signatures using desorption electrospray ionization mass spectrometry. *Anal. Bioanal. Chem.* **404**, 2915–2926 (2012).
72. Sarafian, M. H. et al. Objective set of criteria for optimization of sample preparation procedures for ultra-high throughput untargeted blood plasma lipid profiling by ultra performance liquid chromatography–mass spectrometry. *Anal. Chem.* **86**, 5766–5774 (2014).
73. Ben-David, U. et al. Selective elimination of human pluripotent stem cells by an oleate synthesis inhibitor discovered in a high-throughput screen. *Cell Stem Cell* **12**, 167–179 (2013).

**Publisher's note** Springer Nature remains neutral with regard to jurisdictional claims in published maps and institutional affiliations.

Springer Nature or its licensor (e.g. a society or other partner) holds exclusive rights to this article under a publishing agreement with the author(s) or other rightsholder(s); author self-archiving of the accepted manuscript version of this article is solely governed by the terms of such publishing agreement and applicable law.

© The Author(s), under exclusive licence to Springer Nature Limited 2024

<sup>1</sup>Center for Stem Cell and Regenerative Medicine, Department of Basic Medical Sciences, and Bone Marrow Transplantation Center of the First Affiliated Hospital, Zhejiang University School of Medicine, Hangzhou, China. <sup>2</sup>Liangzhu Laboratory, Zhejiang University, Hangzhou, China. <sup>3</sup>State Key Laboratory of Molecular Developmental Biology, Institute of Genetics and Developmental Biology, Chinese Academy of Sciences, Beijing, China. <sup>4</sup>LipidALL Technologies, Changzhou, China. <sup>5</sup>Center of Reproductive Medicine, Shengjing Hospital of China Medical University, Shenyang, China. <sup>6</sup>NHC Key Laboratory of Advanced Reproductive Medicine and Fertility (China Medical University), National Health Commission, Shenyang, China. <sup>7</sup>College of Biomedical Engineering and Instrument Science, Key Laboratory for Biomedical Engineering of Ministry of Education, Zhejiang University, Hangzhou, China. <sup>8</sup>Institute of Immunology, Department of Surgical Oncology of The First Affiliated Hospital, Zhejiang University School of Medicine, Hangzhou, China. <sup>9</sup>Zhejiang Provincial Key Laboratory for Cancer Molecular Cell Biology, Life Sciences Institute, Zhejiang University, Hangzhou, China. <sup>10</sup>University of Chinese Academy of Sciences, Beijing, China. <sup>11</sup>Center of Gene and Cell Therapy and Genome Medicine of Zhejiang Province, Hangzhou, China. <sup>12</sup>These authors contributed equally: Ling Zhang, Jing Zhao, Sin Man Lam, Lang Chen, Yingzhuo Gao, Wenjie Wang.  e-mail: [leeda@ymail.com](mailto:leeda@ymail.com); [ghshui@genetics.ac.cn](mailto:ghshui@genetics.ac.cn); [zhgene@zju.edu.cn](mailto:zhgene@zju.edu.cn)

## Methods

### Mouse gamete and embryo collection

All experimental procedures were performed in accordance with the Animal Research Committee guidelines of Zhejiang University (research licence ZJU20230458). C57BL/6J mice were housed in the animal facility of Zhejiang University. They were maintained on a 12-h light and 12-h dark cycle. The catalogue number of the diet is 1010085 (Xietong). Female C57BL/6J mice (aged 4–6 weeks), male C57BL/6J mice (aged 8 weeks) and male DBA mice (aged 8 weeks) were purchased from SLAC Animal. All mice had free access to food and water and were maintained in an environment at 22–26 °C with 50–70% humidity on a 12/12-h light–dark cycle.

To collect preimplantation embryos, 4-week-old C57BL/6J female mice were given 7.5 IU of pregnant mare serum gonadotropin (San-Sheng Pharmaceutical) 48 h after injection of 7.5 IU of hCG (San-Sheng Pharmaceutical). The superovulated female mice were mated with C57BL/6J adult male mice overnight after hCG administration. Each set of embryos at a particular stage were flushed from the reproductive tract at defined time periods after hCG administration: 14 h (MII), 24 h (zygote), 48 h (2-cell), 54 h (4-cell), 68 h (8-cell) and 92 h (blastocysts).

### In vitro culture of mouse embryos

PN5-stage zygotes were collected 24 h after hCG administration and cultured in drops of indicated medium (KSOM (Millipore), fatty-acid-free KSOM and BSA-free KSOM (Aibei Biotechnology)) covered by a layer of mineral oil in a humidified incubator at 37 °C, under 5% CO<sub>2</sub>. Zygotes were cultured in medium containing 100 nM CAY10566, 100 nM SC-26196 or 100 nM sesamin for inhibitor treatment, or 100 μM oleic acid, 50 μM EPA or 10 μM ARA for fatty acid supplementation.

### Cell culture

Mouse E14 ESCs were cultured on MEF feeder cells with 1:1 mixture of DMEM/F12 (Gibco, 11320-033) and neurobasal medium (Gibco, 21103-049) supplemented with N2 and B27 (Life Technologies, 17502-048/17504-044), 100 μM non-essential amino acids (Gibco, 11140), 2 mM L-glutamine (Gibco, 25030081), 1,000 U ml<sup>-1</sup> mouse LIF (Pepro-Tech, 250-02), 1 μM PD3259010, 3 μM CHIR99021 (Stem Cell Technologies), 100 μM β-mercaptoethanol (Sigma, M6250), 100 U ml<sup>-1</sup> penicillin and 100 μg ml<sup>-1</sup> streptomycin (Gibco, 15140-122). The medium was changed daily and the cells were routinely passaged every 2 days. For inhibitor treatment, the mouse ESCs were cultured in medium containing 100 nM CAY10566, 100 nM SC-26196 or 100 nM sesamin.

TE stem cells were cultured on MEF feeder cells with PRM11640 (Gibco, 21870-076) containing 20% FBS, 2 mM L-glutamine (Gibco, 25030081), 1 mM sodium pyruvate (Gibco, 11360070), 25 ng ml<sup>-1</sup> FGF4, 1 ng ml<sup>-1</sup> heparin, 100 μM β-mercaptoethanol (Sigma, M6250), 100 U ml<sup>-1</sup> penicillin and 100 μg ml<sup>-1</sup> streptomycin (Gibco, 15140-122). For culture of mouse TSCs, the medium was changed daily and the cells were routinely passaged every 2 days. For inhibitor treatment, the mouse TSCs were cultured in medium containing 100 nM CAY10566, 100 nM SC-26196 or 100 nM sesamin.

### EPSC lines

EPSCs were obtained from J. Yang's laboratory, and the protocol used was the same as previously described<sup>74</sup>. In brief, EPSCs were cultured on MEF feeder cells with DMEM/F12 (Gibco, 11330-032) mixed with 20% KnockOut serum replacement (Gibco, 10828-028) supplemented with 100 μM non-essential amino acids (Gibco, 11140), 1× GlutaMax (Gibco, 35050-061), 10 ng ml<sup>-1</sup> hLIF (PeproTech, 300-05), 3 μM CHIR99021 (Reagents Direct, 27-H76), 1 μM PD0325901 (Selleck Chemicals, S1036), 4 μM JNK inhibitor VII (Millipore, 420135), 10 μM SB203580 (Tocris, 1402), 0.3 μM A-419259 (Tocris, 3914), 5 μM XAV939 (Sigma, X3004) and 0.1 mM β-mercaptoethanol (Sigma, M6250). The medium was changed daily and the cells were routinely passaged every 2 days.

### Generation of EPSC blastoids

The generation of EPSC blastoids was performed as previously described<sup>70</sup>. In brief, EPSC colonies were dissociated into single cells by incubation with TrypLE (Gibco, 12604-021) at 37 °C for 30 min to remove MEF feeder cells. The supernatant containing EPSCs was collected and filtered through a 40 μm cell strainer. Approximately 6,000 cells (5 cells per microwell for 1,200 microwells) were resuspended in EPSC blastoid basal medium supplemented with 2 μM ROCK inhibitor Y-27632 (Reagents Direct, 53-B80-50), 12.5 ng ml<sup>-1</sup> rhFGF4 (R&D, 235F4025), 0.5 μg ml<sup>-1</sup> heparin (Sigma, H3149), 3 μM CHIR99021 (Reagents Direct, 27-H76), 5 ng ml<sup>-1</sup> BMP4 (Proteintech, HZ-1040) and 0.5 μM A83-01 (Axon Medchem, 1421) and seeded into one well of a 24-well AggreWell 400 plate (Stem Cell Technologies, 34415). The plate was centrifuged at 300g for 1 min and placed into an incubator. The day of cell seeding was counted as day 0 of the process. Medium was changed 24 h later and replaced with fresh medium without Y-27632. Starting from day 4, blastoids were manually picked using a mouse pipette under a stereomicroscope for analysis of blastoid formation and downstream immunostaining experiments. EPSC blastoid basal medium was composed of 25% TSC basal medium (PRM11640 medium containing 20% FBS, 2 mM L-glutamine, 1 mM sodium pyruvate and 0.1 mM β-mercaptoethanol), 25% N2B27 basal medium (1:1 mixture of DMEM/F12 and neurobasal medium supplemented with N2 and B27, 100 μM non-essential amino acids, 2 mM GlutaMax and 0.1 mM β-mercaptoethanol) and 50% KSOM (Millipore). For the inhibitor treatment, EPSC blastoid basal medium was supplemented with 100 nM CAY10566, 100 nM SC-26196 or 100 nM sesamin.

### Human embryo collection

**Ethics statement.** The Reproductive Medicine Ethics Committee of Shengjing Hospital approved this study (research licence 2022PS004F) after evaluating its scientific merit and ethical justification, as well as conducting a thorough review of the donation and use of these samples. The research also followed the guidelines of the International Society for Stem Cell Research and was regularly reviewed by The Reproductive Medicine Ethics Committee of Shengjing Hospital. The embryos used in this study were donated by 34 couples who had successfully given birth to healthy offspring through in vitro fertilization. The average age of the female donors was 31 years, and that of the male donor was 38 years old. These couples received proper counselling regarding the research objective, the implications of their donation and potential risks involved. Each participant provided written informed consent for the collection of embryos for research purposes voluntarily, without receiving any compensation.

### Embryo thawing

Both human cleavage-stage and blastocyst-stage embryos were thawed using Kitazato thawing kits (VT102, Shizuoka) in accordance with the manufacturer's instructions. In brief, 1 h before starting the procedure, 1 ml thawing solution (TS) was pre-warmed in a 37 °C incubator. Before starting the thawing procedure, we prepared a 35 mm dish with pre-warmed TS solution and a 4-well dish with diluent solution (DS), washing solution 1 (WS1) and washing solution 2 (WS2) in separate wells (300 μl per well). The straw containing vitrified embryos was removed from liquid nitrogen and quickly immersed into TS for 1 min. Then, the embryos were transferred to the DS and incubated at room temperature for 3 min. Subsequently, the embryos were transferred to WS1 and incubated at room temperature for 5 min, and then to WS2 at room temperature for 5 min.

### Sample preparation for lipid extraction using the one-phase IPA method

The collected oocyte and embryo samples were prepared for lipid extraction as previously described<sup>72</sup>. In brief, the indicated number (120) of embryos at different stages were collected and rinsed in 0.9%

NaCl three times and the samples were precipitated by the addition of 3 volumes of 80% prechilled IPA and mixed by vortexing for 1 min. After incubation for 10 min at room temperature, the samples were stored at -20 °C overnight and then centrifuged at 14,000g for 20 min. The supernatant was transferred to a new Eppendorf tube, dried in a SpeedVac under OH mode and resuspended in appropriate volumes of chloroform and methanol (1:1 v/v) for MS analysis.

### Sample preparation for lipid extraction using the Bligh&Dyer method

For oocyte and embryo collection for lipidomics analysis, the indicated number (120) of embryos at different stages were collected and rinsed in 0.9% NaCl three times and lysed in 250 µl of ice-cold methanol on dry ice. All collected oocytes and embryos were kept at -80 °C before extraction. The samples in ice-cold methanol were transferred to 2-ml glass vials, then topped up with another 250 µl of ice-cold methanol, 250 µl of ice-cold chloroform and 75 µl of LCMS-grade water based on a modified version of the Bligh&Dyer method, as previously described<sup>52</sup>. Then, the samples were incubated at 2,000 r.p.m. for 30 min at 4 °C. At the end of the incubation period, the samples were centrifuged to obtain clear phase separation, and the lower organic (chloroform) phase containing lipids was extracted into a clean glass vial. Lipid extraction was repeated once by adding 500 µl of chloroform to the remaining biological material in the aqueous phase, and the lipid extracts were pooled into a single glass vial and dried in a SpeedVac under OH mode. Samples were stored at -80 °C until further analysis.

### Lipidomics analysis

Polar lipids were analysed using a Shimadzu UPLC connected to a 7500 QTRAP system (SCIEX), with methodological details comprehensively reported in a previous publication<sup>75</sup>. Separation of individual lipid classes of polar lipids by normal phase (NP) HPLC was carried out using a TUP HB silica 3 µm column (internal diameter 150 × 3.0 mm) with the following conditions: mobile phase A (chloroform, methanol and ammonium hydroxide at 89.5:10:0.5 ratio) and mobile phase B (chloroform, methanol, ammonium hydroxide and water at 55:39:0.5:5.5 ratio). MRM transitions were set up for analysis of various polar lipids. Quantitative analysis of lipidomics was performed as previously reported<sup>52,76–78</sup>. Individual lipid species were quantified by referencing to spiked internal standards, which included d<sub>9</sub>-PC32:0(16:0/16:0), d<sub>7</sub>-PE33:1(15:0/18:1), d<sub>7</sub>-PG33:1(15:0/18:1), d<sub>31</sub>-PS(16:0/18:1), d<sub>7</sub>-PI33:1(15:0/18:1), d<sub>9</sub>-PC18:0p/18:1, d<sub>9</sub>-PE18:0p/18:1, C14-BMP, d<sub>9</sub>-SM d18:1/18:1, C15 ceramide-d<sub>1</sub>(d18:1-d<sub>7</sub>/15:0), C8-GluCer, C8-GalCer, d<sub>3</sub>-LacCer d18:1/16:0, C17-SL, GM3-d18:1/18:0-d<sub>3</sub>, Gb3 d18:1/17:0, d<sub>7</sub>-LPC18:1, d<sub>7</sub>-LPE18:1 and d<sub>5</sub>-CL72:8(18:2)<sub>4</sub> from Avanti Polar Lipids and d<sub>3</sub>-16:0-carnitine from Cambridge Isotope Laboratories. Glycerol lipids including DAGs and TAGs were quantified using a modified version of reverse-phase HPLC/MRM. Separation of neutral lipids was achieved using a Phenomenex Kinetex-C18 2.6 µm column (i.d. 4.6 × 100 mm) using an isocratic mobile phase containing chloroform, methanol and 0.1 M ammonium acetate (100:100:4 v/v/v) at a flow rate of 170 µl. Levels of short-chain, medium-chain and long-chain TAGs were calculated by referencing to spiked internal standards of TAG(14:0)<sub>3</sub>-d<sub>5</sub>, TAG(16:0)<sub>3</sub>-d<sub>5</sub> and TAG(18:0)<sub>3</sub>-d<sub>5</sub> obtained from CDN isotopes, respectively. DAGs were quantified using d<sub>5</sub>-DAG17:0/17:0 and d<sub>5</sub>-DAG18:1/18:1 as internal standards (Avanti Polar Lipids). Free cholesterol and cholestry esters were analysed as previously described with d<sub>6</sub>-cholesterol and d<sub>6</sub>-C18:0 cholestry ester (CDN isotopes) as internal standards<sup>79</sup>. Free fatty acids were quantified using d<sub>31</sub>-16:0 (Sigma-Aldrich) and d<sub>8</sub>-20:4 (Cayman Chemicals) as internal standards.

### Immunofluorescence analysis by confocal microscopy

Embryos were fixed in 4% paraformaldehyde for 20 min at room temperature, washed three times in PBS with 3 mg ml<sup>-1</sup> polyvinylpyrrolidone (PVP-PBS, Sigma, PVP-360), permeabilized in PBS with 0.25%

Triton X-100 for 1 h at room temperature and incubated in blocking solution (0.2% BSA, 0.25% Triton X-100, 0.01% Tween 20, 2% donkey serum and 3 mg ml<sup>-1</sup> PVP in PBS) for 1 h. Then, the embryos were incubated at 4 °C overnight in primary antibodies diluted in blocking solution at the following concentrations: K8 (DSHB, TROMA-I) at 1:20; K18 (Sigma, SAB4501665) at 1:200; NANOG (R&D, AF2729) at 1:200; CDX2 (Biogenex, AM392-5M, the anti-CDX2 antibody is a ready-to-use antibody with no need to further dilute according to the manufacturer's instructions); αPKC at 1:50 (Santa Cruz, 17781); E-cadherin at 1:100 (Sigma, U3254); ezrin at 1:100 (Cell Signaling Technology, 3145S); phosphorylated ezrin at 1:100 (Cell Signaling Technology, 3726T); and YAP at 1:100 (Cell Signaling Technology, 8418S). After incubation with primary antibodies, embryos were washed three times in blocking solution and then incubated for 1 h at room temperature with a secondary antibody (Alexa Fluor 647, ab150075; Alexa Fluor 488, ab150061) diluted in blocking solution to 1:400, followed by washing three times with blocking solution. Then, nuclei were stained with DAPI for 10 min, and the samples were washed three times before mounting in PVP-PBS covered with mineral oil (Sigma, M8410) in a glass-bottom cell culture dish. Imaging was performed using an Olympus FV3000 fluorescence microscope at ×60 magnification with an oil-immersion objective.

### PE staining

Different stages of embryos were collected at specific time periods after injection of hCG as described above. Live embryos were incubated with 0.2 µM duramycin-LC-biotin (Molecular Targeting Technologies, D-1003) diluted in KSOM medium at 37 °C for 1 h, fixed in 4% paraformaldehyde for 20 min, permeabilized in PBS with 0.25% Triton X-100 for 1 h at room temperature and then incubated with Alexa Fluor 647-conjugated streptavidin (Invitrogen, 2352166) for 1 h, followed by washing three times in blocking solution. Nuclei were stained with DAPI for 10 min, and embryos were washed three times before mounting in PVP-PBS covered with mineral oil in a glass-bottom cell culture dish.

### Lipid raft staining

Different stages of embryos were collected at specific time periods after injection of hCG as described above. Live embryos were washed three to four times with 0.3% PVP-PBS. A lipid raft labelling kit (Thermo Fisher, V34404) was used to stain the pentasacharide chain of the plasma membrane ganglioside GM1, which selectively partitions into lipid rafts<sup>80</sup>. In brief, live embryos were incubated with 1 µg ml<sup>-1</sup> working solution at 4 °C for 10 min, then washed three times with cold 0.3% PVP-PBS. Incubation with secondary antibody was performed at 4 °C for 15 min, then washed three times with cold 0.3% PVP-PBS. Embryos were fixed in 4% paraformaldehyde for 20 min at room temperature, washed three times with 0.3% PVP-PBS and permeabilized in PBS with 0.25% Triton X-100 for 10 min at room temperature. Nuclei were stained with DAPI for 10 min, and the samples were washed three times before mounting in PVP-PBS covered with mineral oil in a glass-bottom cell culture dish.

### FRAP analysis

Different stages of embryos were collected at specific time periods after injection of hCG as described above. Zona pellucidas were removed using pronase (Sigma) at 37 °C for about 10 min. Embryos were stained using a Cell Plasma Membrane Staining kit with Dil (Beyotime), a lipophilic carbocyanine dye that can label live embryo plasma membrane. The dilution and incubation time were according to the manufacturer's instructions. After membrane staining, embryos were washed in Hanks' balanced salt solution three times followed by nuclei staining with Hoechst (Sigma). Embryo membrane fluidity was measured using FRAP analysis as previously described<sup>81</sup>. FRAP experiments were performed on a Zeiss (Jena) LSM800 confocal laser scanning microscope equipped with a ×40/NA 1.20 objective at ×1 zoom magnification maintained at 37 °C and 5% CO<sub>2</sub>. A 5 × 10 µm region of interest (ROI) and an identical background region were set using ZEN system software. The ROI was

photobleached with 100% laser power at 561 nm, and the fluorescent signal was monitored every 5 s for a total of 60 cycles. Fluorescence intensity was corrected by background fluorescence and normalized to the pre-bleaching intensity. A fluorescent recovery curve was fitted with a single exponential model using GraphPad software.

### Image analysis

Image analysis was performed using Imaris9. 3D segmentation of whole embryos was performed using the Imaris manual surface rendering module. To determine the fluorescence intensity between cell–cell contacts for K8, K18 and E-cadherin, the regions of cell–cell contact of the same size were cropped, and the mean signal was extracted using the Fiji ROI function. For the intensity of NANOG, CDX2 and YAP, the nuclear region of the specific protein was calculated using the Fiji ROI function. For analysis of phosphorylated ezrin enrichment at the apical domain, a previously published calculation method was used<sup>68</sup>, in which a freehand line was drawn along the apical domain and the signal intensity was calculated using the Fiji ROI function.

### Calculation of diversity score

We used the Shannon diversity index to measure the species diversity of lipids during preimplantation development. The index ( $D$ ) was calculated using the following formula:

$D = -\sum(p_i \times \ln p_i)$ , where sum is the total number of lipid species detected,  $i$  represents the subclass of lipids (such as PCs and PEs) and  $p_i$  is the proportion of abundance of a subclass of lipid relative to the total amount of lipids<sup>40</sup>.

### Microinjection of siRNAs to embryos

In total, 20  $\mu$ M of pooled siRNA solution was injected into the cytoplasm of zygotes using an Eppendorf FemtoJet and Narishige micromanipulators. The microinjected zygotes were further cultured at 37 °C under 5% CO<sub>2</sub> up to the blastocyst stage. Information regarding siRNAs is provided in Supplementary Table 5.

### mRNA preparation and microinjection of mRNAs to embryos

Plasmids for ezrin-mCherry and phalloidin-GFP were linearized by restriction enzymes and transcribed in vitro using a mMESSAGE mMA-CHINE kit (Thermo Fisher, AM1340). mRNAs were purified using lithium chloride precipitation. Microinjection was performed using an Eppendorf FemtoJet and Narishige micromanipulators, with zygotes cultured in M2 medium on a Petri dish and covered with mineral oil. mRNAs were injected at a concentration of 400 ng  $\mu$ l<sup>-1</sup> for ezrin-mCherry and phalloidin-GFP.

### Embryo mRNA extraction

Embryos (5 embryos per sample) were collected in a 0.2 ml PCR tube, and 4  $\mu$ l of lysis buffer (0.2% Triton X-100, RNase inhibitor, dNTP and oligo-dT primers) was added. The samples were immediately incubated at 72 °C for 3 min, and complementary DNA was made using Superscript II reverse transcriptase.

### Embryo transfer experiments

Embryos were cultured in BSA-free KSOM medium until day E4.0. At 3–4 h before the experiments, embryos were transferred to fresh BSA-free KSOM medium. Subsequently, embryos were transferred into the uterine horns of E2.5 pseudopregnant female mice. E7.5 deciduae were explanted 5 days after transfer. The bulb showing a bigger width than a normal uterus was considered as a decidua.

### RNA-seq library preparation and sequencing

The RNA-seq libraries were generated from early mouse embryos using the Smart-seq2 protocol as previously described, with minor modifications<sup>82</sup>. Embryos were collected (5 embryos) in a 0.2 ml PCR tube and lysed in lysis buffer (0.2% Triton X-100, RNase inhibitor, dNTP

and oligo-dT primers). After incubation at 72 °C for 3 min, cDNA was made using Superscript II reverse transcriptase. The cDNA was amplified using KAPA HiFi HotStart with -12 cycles. Sequencing libraries were constructed from 1 ng of preamplified cDNA using a DNA library preparation kit (TruePrep DNA Library Prep Kit V2 for Illumina, Vazyme). Libraries were sequenced on a HiSeq PE150 according to the manufacturer's instructions.

### Next-generation sequencing data analysis

The RNA-seq raw data in fastq format were first processed to obtain clean data using fastp v.0.23.2 software with the default parameters to trim reads containing adapters and to filter low-quality reads and reads containing N bases. The clean data were aligned to the GRCm39 (UCSC) genome assemblies using STAR v.2.7.10a software with default parameters, and the uniquely mapped read pairs were counted using featureCounts v.2.0.1 software. The output gene count matrix was quantile-normalized using the R package DESeq2 v.1.32.0, and rlog transformation of the count matrix was performed for PCA. Significance and fold change of differential expression genes between siNC and siScd1 samples were estimated using the R package DESeq2, and genes with FDR < 5% and the absolute value of log<sub>2</sub>(FC) ≥ 1 were selected. Based on these genes, enriched Gene Ontology biological process terms were then acquired using gene set enrichment analysis with default parameters.

### Statistics and reproducibility

Statistical analyses and data presentation were performed in GraphPad Prism v.9.0.0. The number of independent experiments are listed in the corresponding figure legends. Unpaired two-tailed Student's *t*-test and chi-squared test were used when two groups were compared, and exact *P* values are provided in the corresponding figures. All the findings were reproducible over multiple independent experiments within a reasonable degree of variability between replicates. No statistical methods were used to predetermine sample sizes, but our sample sizes were similar to those reported in previous publications<sup>10</sup>. No data were excluded from the analyses. Data distribution was assumed to be normal, but this was not formally tested. The experiments were not randomized, and the investigators were not blinded to allocation during outcome assessment.

### Reporting summary

Further information on research design is available in the Nature Portfolio Reporting Summary linked to this article.

### Data availability

Sequencing data have been deposited into the Gene Expression Omnibus (GEO) under accession code [GSE213782](#). Previously published RNA-seq data<sup>4</sup> that were re-analysed here are available at the GEO under accession code [GSE98150](#). All other data supporting the findings of this study are available from the corresponding authors on reasonable request. Source data are provided with this paper.

### References

74. Yang, J. et al. Establishment of mouse expanded potential stem cells. *Nature* **550**, 393–397 (2017).
75. Miao, H. et al. Lipidome atlas of the developing heart uncovers dynamic membrane lipid attributes underlying cardiac structural and metabolic maturation. *Research* **2022**, 0006 (2022).
76. Song, J. W. et al. Omics-driven systems interrogation of metabolic dysregulation in COVID-19 pathogenesis. *Cell Metab.* **32**, 188–202, e5 (2020).
77. Lam, S. M. et al. Quantitative lipidomics and spatial MS-imaging uncovered neurological and systemic lipid metabolic pathways underlying troglomorphic adaptations in cave-dwelling fish. *Mol. Biol. Evol.* **39**, msac050 (2022).

78. Lam, S. M., Tian, H. & Shui, G. Lipidomics, en route to accurate quantitation. *Biochim. Biophys. Acta Mol. Cell Biol. Lipids* **1862**, 752–761 (2017).
79. Shui, G. et al. Derivatization-independent cholesterol analysis in crude lipid extracts by liquid chromatography/mass spectrometry: applications to a rabbit model for atherosclerosis. *J. Chromatogr. A* **1218**, 4357–4365 (2011).
80. Merritt, E. A., Sixma, T. K., Kalk, K. H., van Zanten, B. A. & Hol, W. G. Galactose-binding site in *Escherichia coli* heat-labile enterotoxin (LT) and cholera toxin (CT). *Mol. Microbiol.* **13**, 745–753 (1994).
81. Yu, H. et al. rRNA biogenesis regulates mouse 2C-like state by 3D structure reorganization of peri-nucleolar heterochromatin. *Nat. Commun.* **12**, 6365 (2021).
82. Picelli, S. et al. Full-length RNA-seq from single cells using Smart-seq2. *Nat. Protoc.* **9**, 171–181 (2014).

## Acknowledgements

We thank members of J. Zhang's laboratory and Dr. X. Huang for discussions and help with paper preparation; Y. Ding and S. Hong from the animal core facilities of Zhejiang University School of Medicine for their technical support; and Z. Lin and L. Xuan from the Core Facilities, Zhejiang University School of Medicine for their technical support. This work was funded by the National Natural Science Foundation of China (91857116, 82373238 and 31871453 to J. Zhang), the National Key Research and Development Program of China (2018YFA0107103 and 2018YFC1005002 to J. Zhang), a Zhejiang Innovation Team grant (2019R01004 to J. Zhang), the Zhejiang Natural Science Foundation (LR19C120001 to J. Zhang), the Key Research and Development Program of Zhejiang Province (2023C03036 to J. Zhang), the National Natural Science Foundation of China (92057202 to G.S.) and the National Natural Science Foundation projects of China (32000809 to L.Z.).

## Author contributions

L.Z. and J. Zhang conceived and designed the experiments. L.Z., L.C., J. Zhao and W.W. collected mouse oocytes and early-stage embryos. Y.G. collected human embryos. S.M.L. performed lipidomics and W.W. performed blastoid experiments. L.Z., J. Zhao, W.W., Y.X., T.T., M.Z., X.L., M.W. and J.H. performed other experiments. L.Z., H.Y., B.L. and T.Z. performed bioinformatics analyses. L.Z. and J. Zhang wrote the paper with discussion from G.S., D.L., C.Y., N.S., H.J.L. and Q.D.Z.

## Competing interests

S.M.L. and B.L. are employees of LipidALL Technologies. The other authors declare no competing interests.

## Additional information

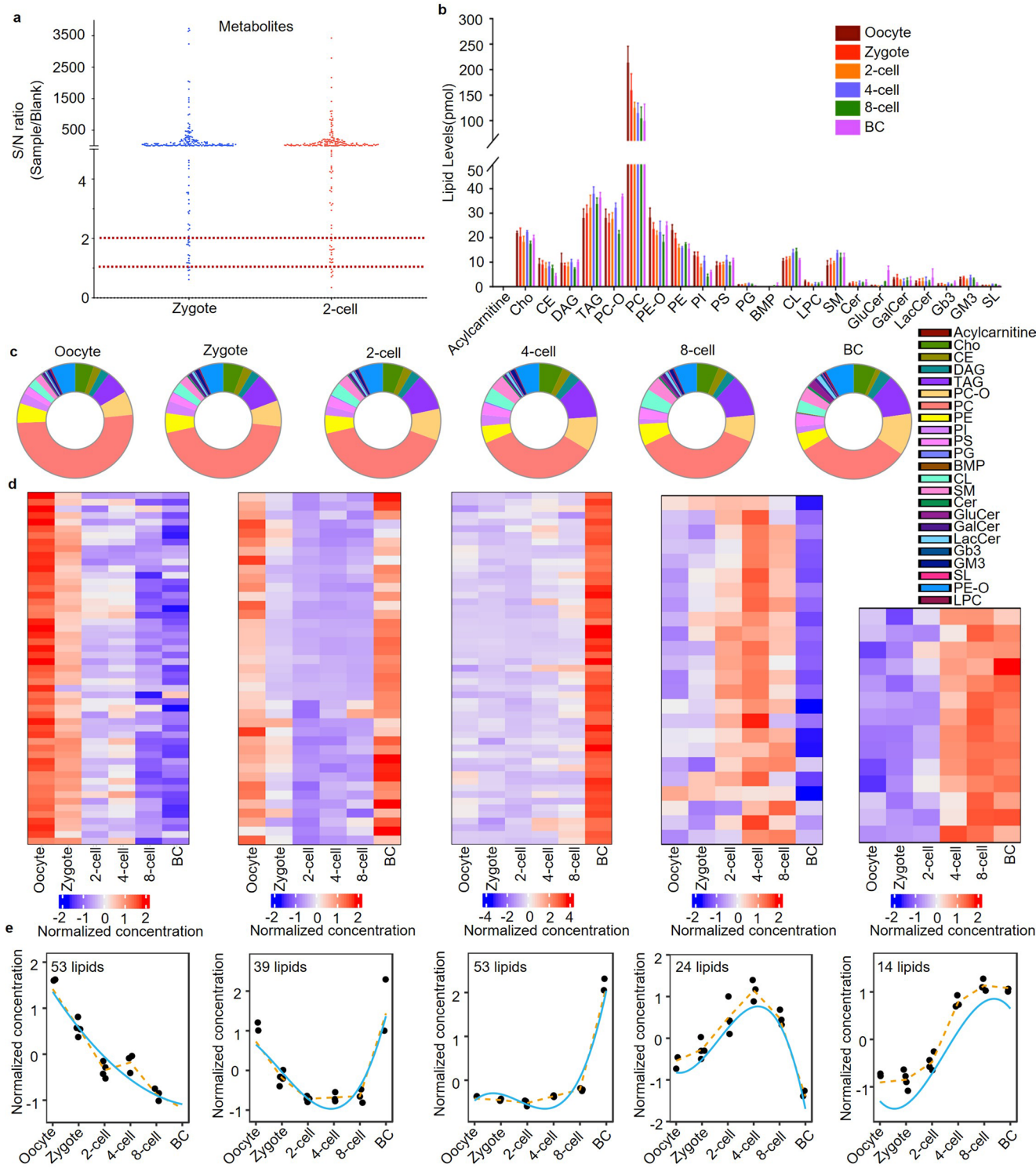
**Extended data** is available for this paper at  
<https://doi.org/10.1038/s41556-023-01341-3>.

**Supplementary information** The online version contains supplementary material available at  
<https://doi.org/10.1038/s41556-023-01341-3>.

**Correspondence and requests for materials** should be addressed to Da Li, Guangzhou Shui or Jin Zhang.

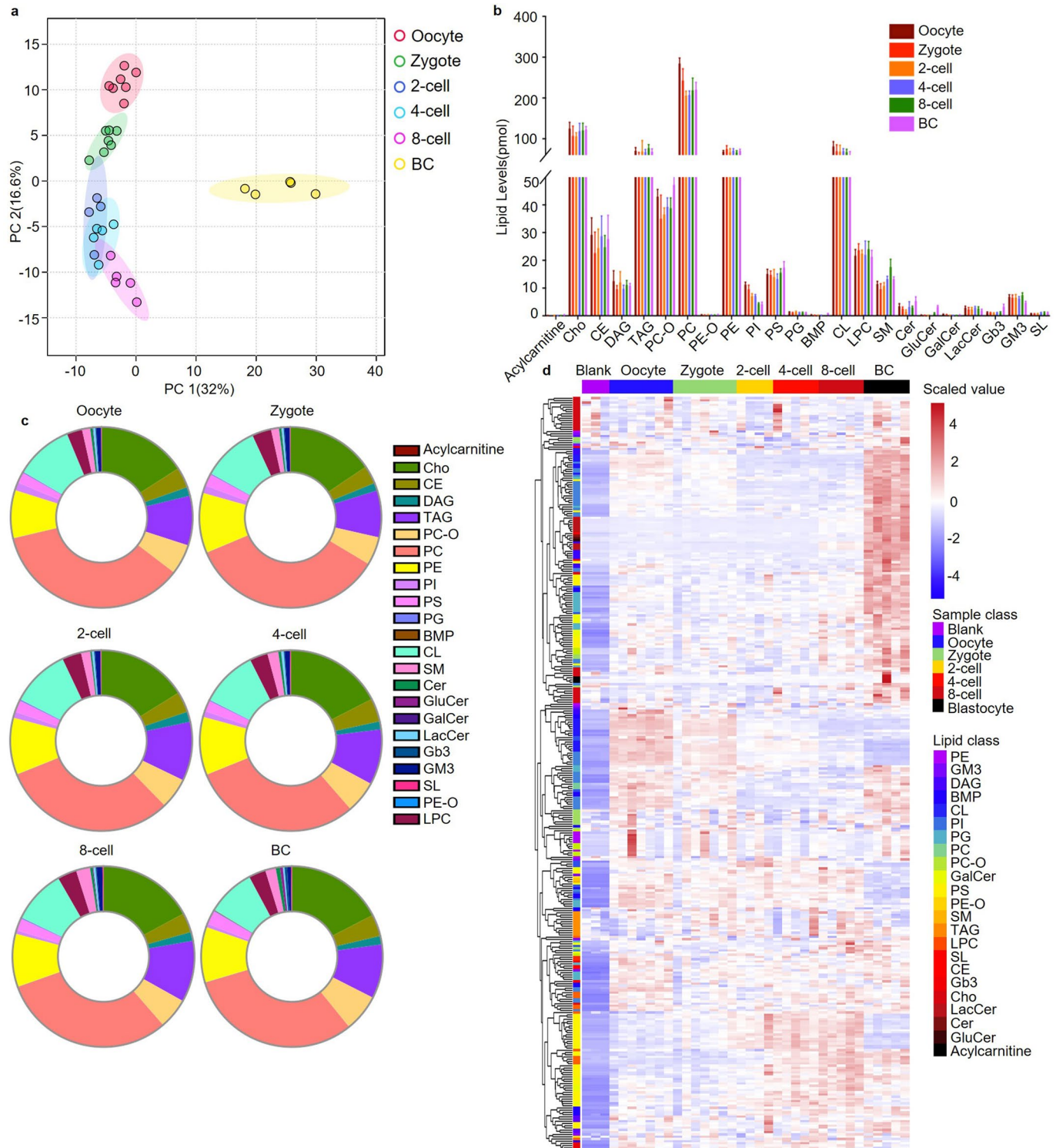
**Peer review information** *Nature Cell Biology* thanks Satoshi Tsukamoto and the other, anonymous, reviewer(s) for their contribution to the peer review of this work. Peer reviewer reports are available.

**Reprints and permissions information** is available at  
[www.nature.com/reprints](http://www.nature.com/reprints).



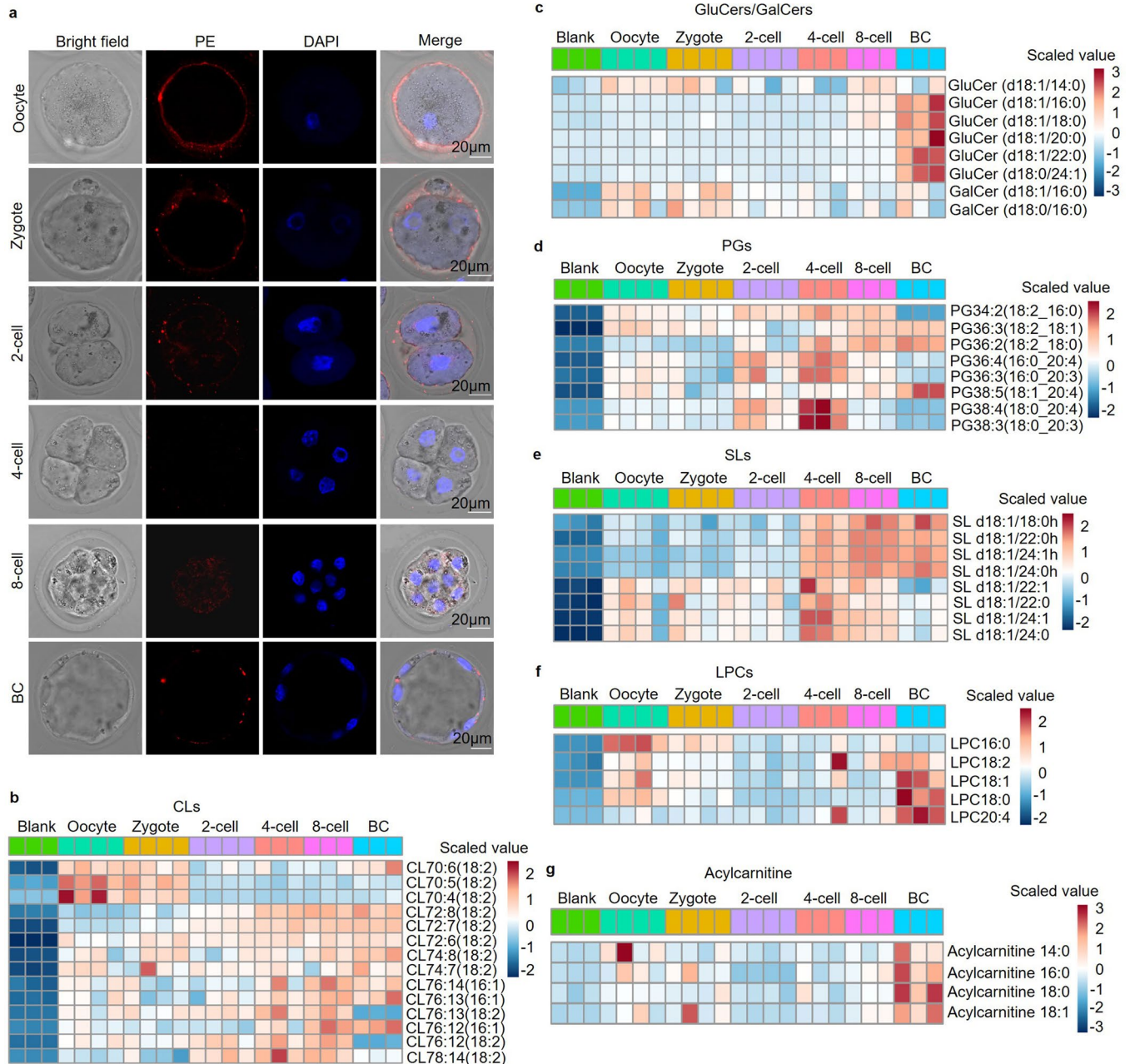
**Extended Data Fig. 1 | Dynamic changes of lipidome in mouse preimplantation embryo development.** (a) A total of 120 zygotes and 120 two-cell embryos were used for embryos number testing in a lipidomic experiment. The ratio of sample/blank represents the sample signal/noise value. The dots (blue or pink) represent metabolites detected. (b) Levels of all lipid classes quantified by LC-MS in six developmental stages. Data are from four biological replicates of oocytes, zygote and two-cell stage embryos each and three biological replicates of four-cell, eight-cell and blastocyst stage embryos each and are presented as the mean  $\pm$  s.e.m. (c) A pie chart showing

the proportion of each lipid class in every developmental stage. (d) Heatmaps showing distinct temporal patterns of lipids along the six developmental stages. Data are from averaged lipid concentrations in each stage of the same biological replicates in (b). (e) Linear plots showing the trends of lipid clusters along the six developmental stages. Black dots represent the averaged Z-scores of the concentration of clustered lipids in the six developmental stages, yellow lines connect the median points of all the samples at each developmental stage, and blue curves represent the fitted levels by the maSigPro model.



**Extended Data Fig. 2 | Dynamic changes of lipidome in mouse preimplantation embryo development using the Bligh & Dyer method.** (a) A PCA plot of the lipidomics profiling data showing clustering of seven biological replicates of oocytes and zygote stage embryos each, four biological replicates of two-cell stage embryos each and five biological replicates of four-cell, eight-cell and blastocyst stage embryos each. (b) Levels of all lipid classes quantified by LC-

MS in six developmental stages. Data are from the same biological replicates as in (a) and are presented as the mean +/- s.e.m. (c) A pie chart showing the proportion of each lipid class in every developmental stage. (d) Heatmaps showing the relative abundance of lipids in oocytes, zygotes, two-cell, four-cell, eight-cell and blastocyst embryos. Scaled value bar indicates the relative concentration. Data are from the same biological replicates as in (a).



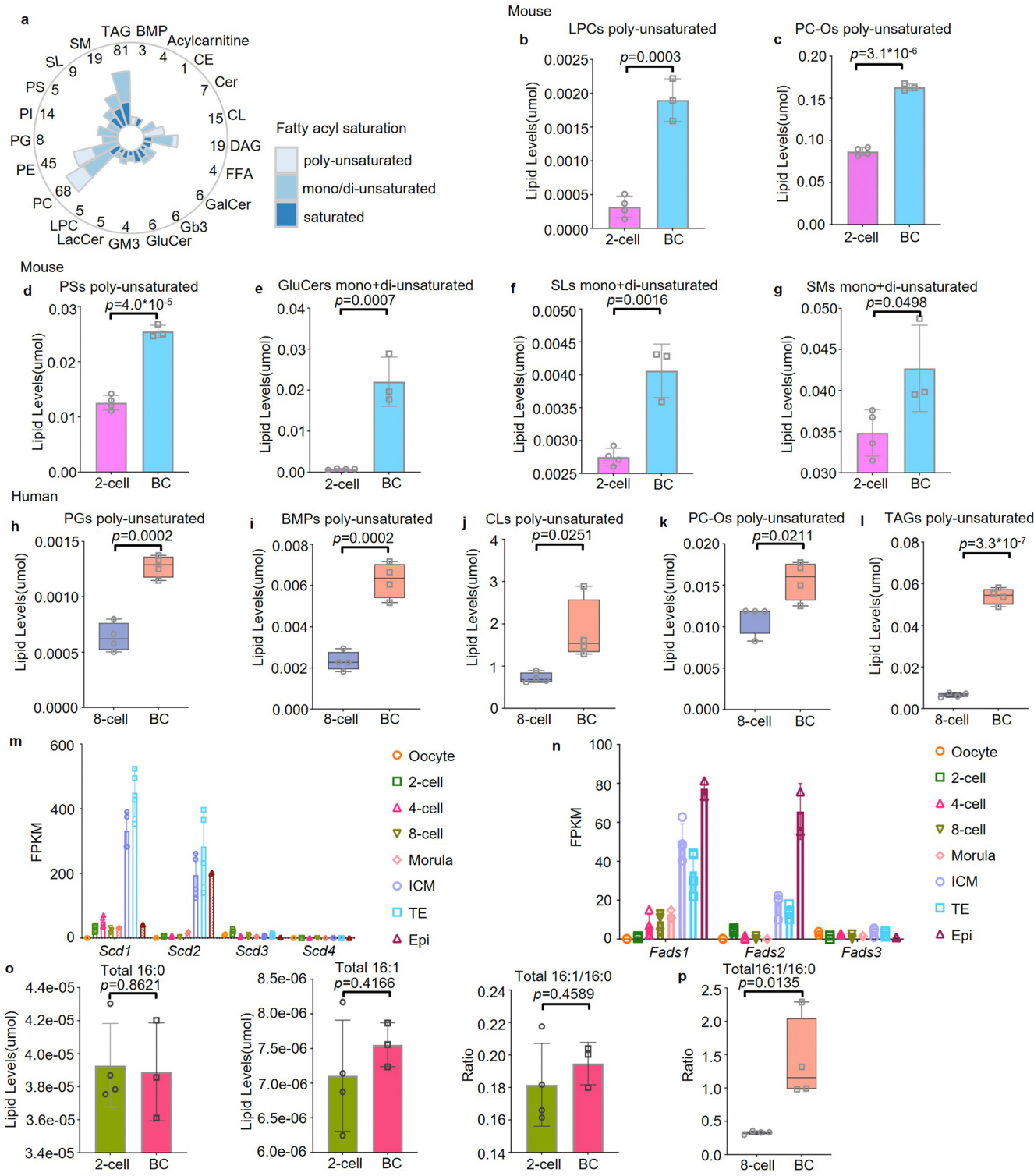
**Extended Data Fig. 3 | Dynamic changes of different lipid classes during mouse preimplantation embryo development support lipid-mediated functions.** (a) Immunofluorescence of PEs staining showing its dynamic change in abundance in the six developmental stages. (b-g) A heatmap of individual species CLs (b), GluCers (c), PGs (d), SLs (e), LPCs (f) and acylcarnitine (g)

quantified by LC-MS in six developmental stages. Scaled value bar indicates relative concentration. Data are from four biological replicates of oocytes, zygote and two-cell stage embryos each and three biological replicates of four-cell, eight-cell and blastocyst stage embryos each.



**Extended Data Fig. 4 | Dynamic changes of individual lipid classes during mouse preimplantation embryo development using the Bligh & Dyer method.** (a-h), Heatmaps showing the levels of each class of species of PCs (a), PIs (b), PC-Os (c), Gb3 (d), GluCers (e), SMs (f), TAGs (g) and CE and Cho (h) in six

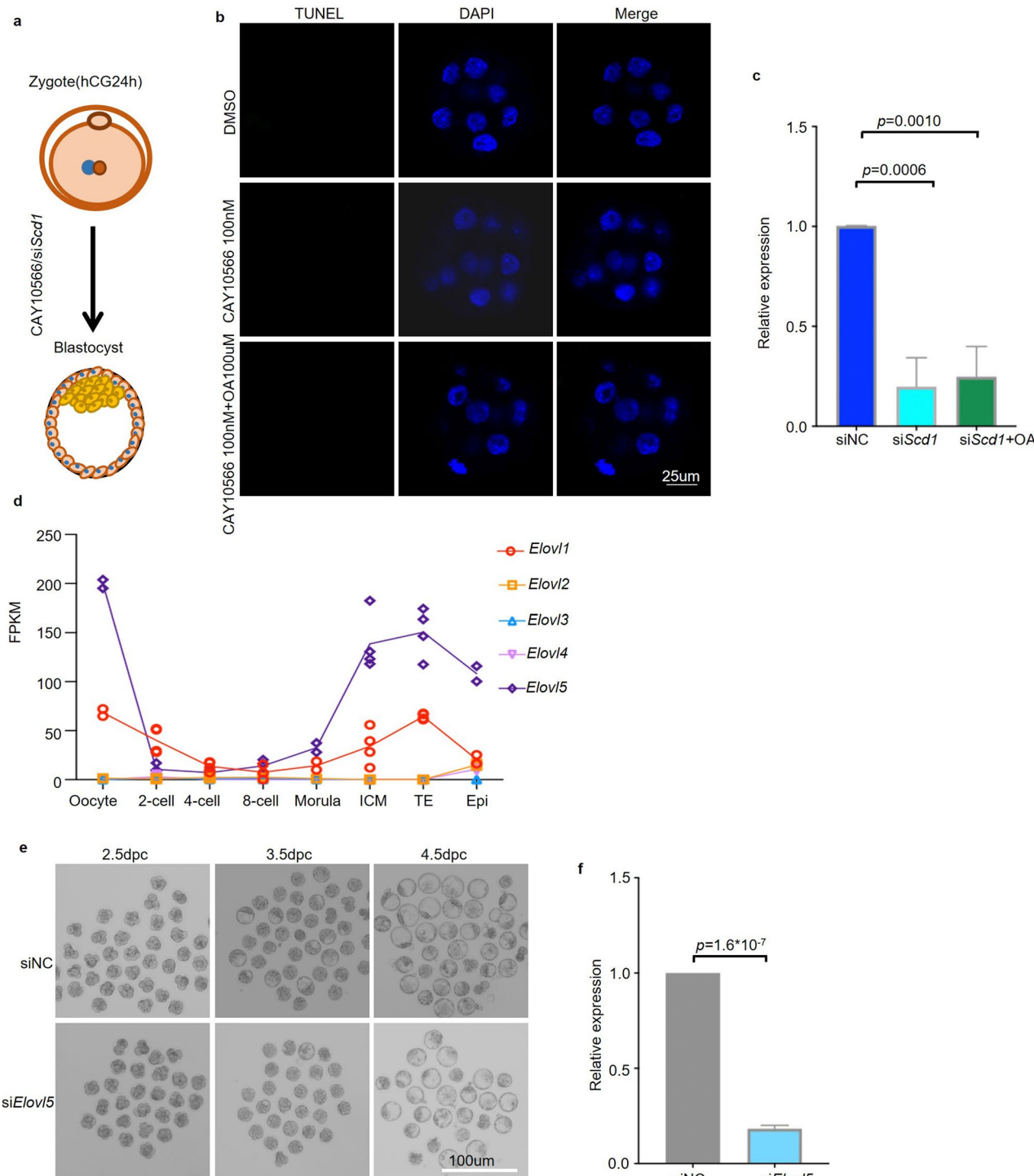
developmental stages. Scaled value bar indicates relative concentration. Data are from seven biological replicates of oocytes, zygote stage embryos each, four biological replicates of two-cell stage embryos and three biological replicates of four-cell, eight-cell and blastocyst stage embryos each.



Extended Data Fig. 5 | See next page for caption.

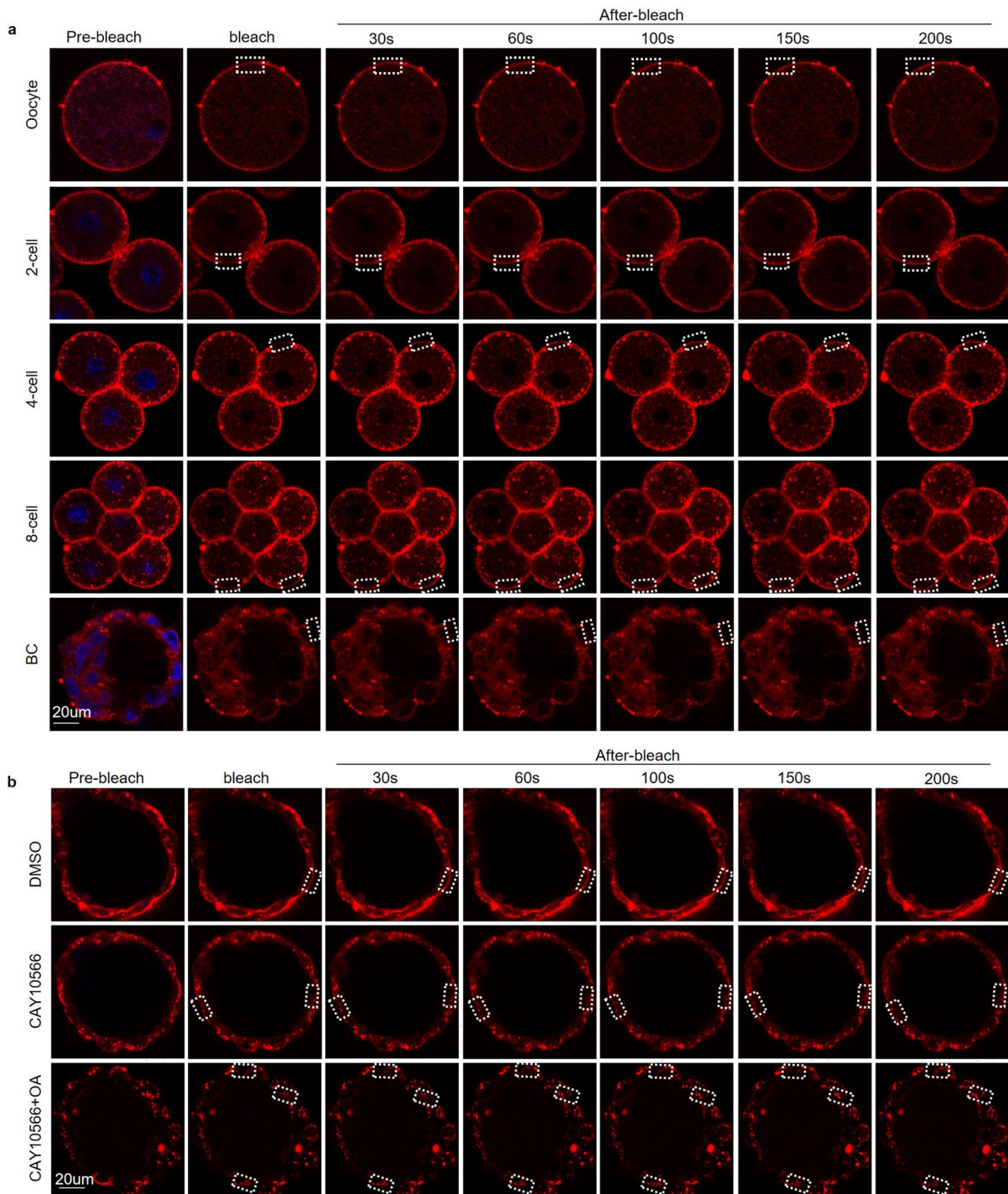
**Extended Data Fig. 5 | The degree of lipid unsaturation is increased during mammalian preimplantation embryo development.** (a) Nightingale rose chart showing the distribution of polyunsaturated, mono+diunsaturated and saturated lipids in different lipid classes. Numbers of species measured in each class are shown. (b-d) Bar graphs showing the polyunsaturated lipid levels of LPCs (b), PC-Os (c) and PSs (d) in the mouse two-cell and blastocyst stage embryos. (e-g) Bar graphs showing the mono+diunsaturated lipid levels of GluCers (e), SLs (f) and SMs (g) in the mouse two-cell and blastocyst stage embryos. (h-l) Box plots showing the polyunsaturated lipid levels of PGs (h), BMPs (i), CLs (j), PC-Os (k) and TAGs (l) in the human eight-cell and blastocyst stage embryos. (m-n) FPKM values of *Scd* gene (m) and *Fads* gene (n) transcripts at different developmental stages. Each dot represents one biological replicate. Data are from two biological replicates of oocytes, four biological replicates of two-cell and four-cell stage embryos, three biological replicates of eight-cell stage embryos, two biological replicates of morula stage embryos, four

biological replicates of ICM and TE of E3.5 blastocyst stage embryos, and two biological replicates of Epi of E6.5 of post-implantation embryos (ref. 4) and are presented as the mean +/- s.e.m. (o) Bar graphs illustrating the levels of palmitic acid (C16:0), palmitoleic acid (C16:1) and the ratio of C16:1/C16:0 in the mouse two-cell and the blastocyst stage embryos. (p) Box plot showing the ratio of palmitoleic acid (C16:1)/palmitic acid (C16:0) in the human eight-cell and blastocyst stage embryos. (b-g, o) Each dot represents one biological replicate, and data are from four biological replicates of two-cell stage embryos each and three biological replicates of blastocyst stage embryos each and are presented as the mean +/- s.e.m. Statistical significance was determined by two-tailed unpaired *t* test. (h-l, p) Each dot represents one biological replicate, data are from four biological replicates of eight-cell and blastocyst stage embryos each and are presented as the mean +/- s.e.m. Statistical significance was determined by two-tailed unpaired *t* test. Center line, median; box, 25th and 75th percentiles, whiskers, 1.5xIQR.

**Extended Data Fig. 6 | Inhibition of SCD1 during mouse embryo development.**

(a) A schematic of the experimental approach. Zygotes were isolated at 24 h after injection of hCG and cultured in KSOM medium with 100 nM CAY10566 or 100 nM CAY10566 plus 100 nM oleic acid, or *Scd1* siRNA injection was performed at the zygote stage, and the embryos were collected at the indicated times for further analysis. (b) TUNEL assay was performed at 3.5 d.p.c embryos cultured in medium with DMSO, 100 nM CAY10566 or 100 nM CAY10566 plus 100 nM oleic acid. Representative images of embryos under the above three conditions are shown. (c) *Scd1* mRNA expression at 3.5 d.p.c after *Scd1* siRNA injection at the zygote stage. Data are from three independent experiments and are presented as the mean +/- s.e.m. Statistical significance was determined by two-tailed unpaired *t* test. (d) FPKM values of *Elov1*–*Elov5* gene transcripts at different developmental

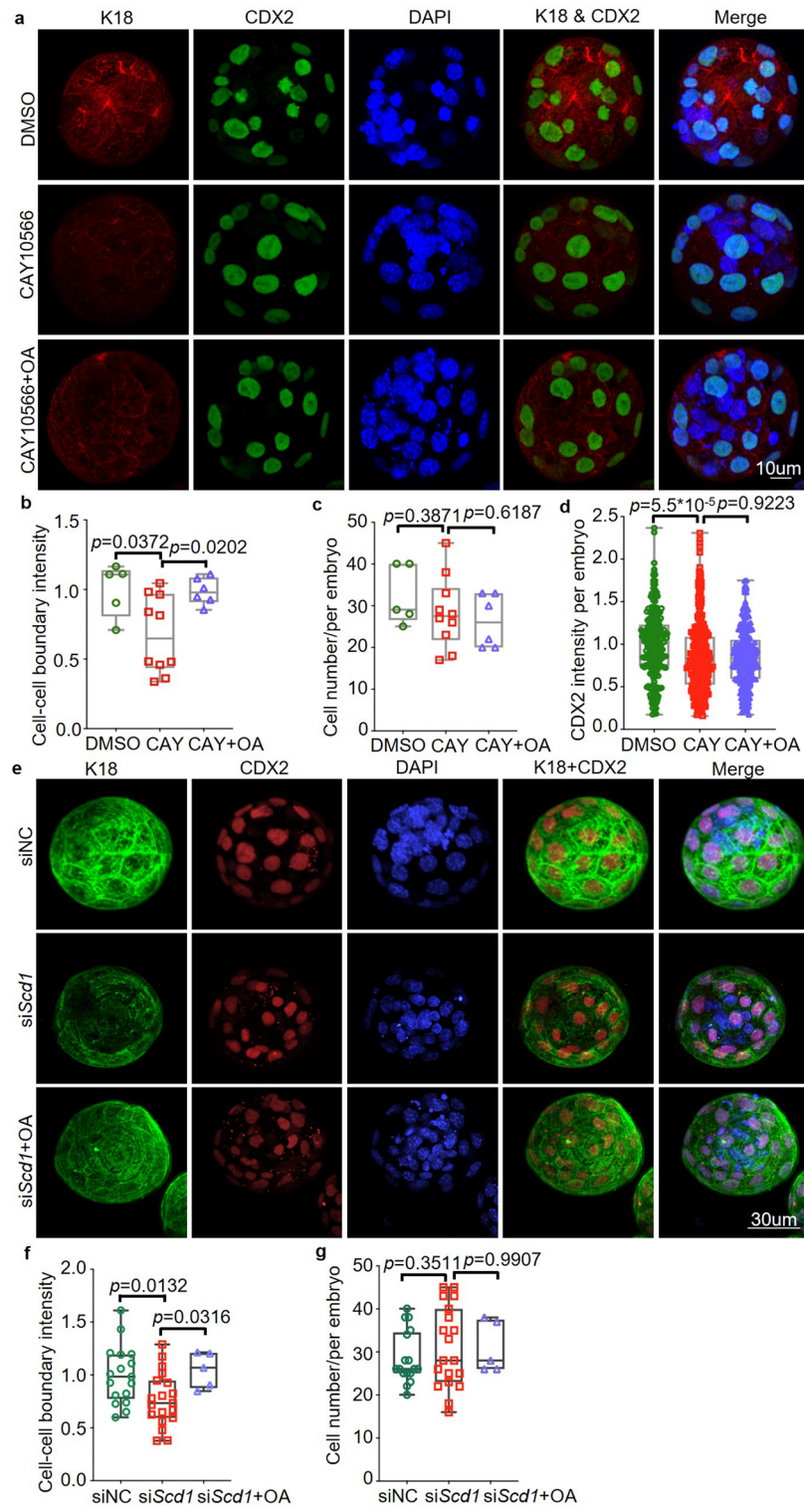
stages. Each dot represents one biological replicate. Data are from two biological replicates of oocytes, four biological replicates of two-cell and four-cell stage embryos, three biological replicates of eight-cell stage embryos, two biological replicates of morula stage embryos, four biological replicates of ICM and TE of E3.5 blastocyst stage embryos, and two biological replicates of Epi of E6.5 of post-implantation embryos (ref. 4) and are presented as the mean +/- s.e.m. (e) Representative images of mouse embryos at 2.5, 3.5 or 4.5 d.p.c that were treated with siRNA of scramble (NC) or *Elov5* from the zygote stage. The images shown are representative of three independent experiments. (f) *Elov5* mRNA expression at 4.5 d.p.c after *Elov5* siRNA injection at the zygote stage. Data are from three independent experiments and are presented as the mean +/- s.e.m. Statistical significance was determined by two-tailed unpaired *t* test.



**Extended Data Fig. 7 | The lipid desaturase SCD1 mediates cell plasma membrane fluidity in mouse preimplantation embryo development.**

(a) FRAP analysis showing recovery after photobleaching to indicate cell membrane fluidity in embryos of all developmental stages. The images shown

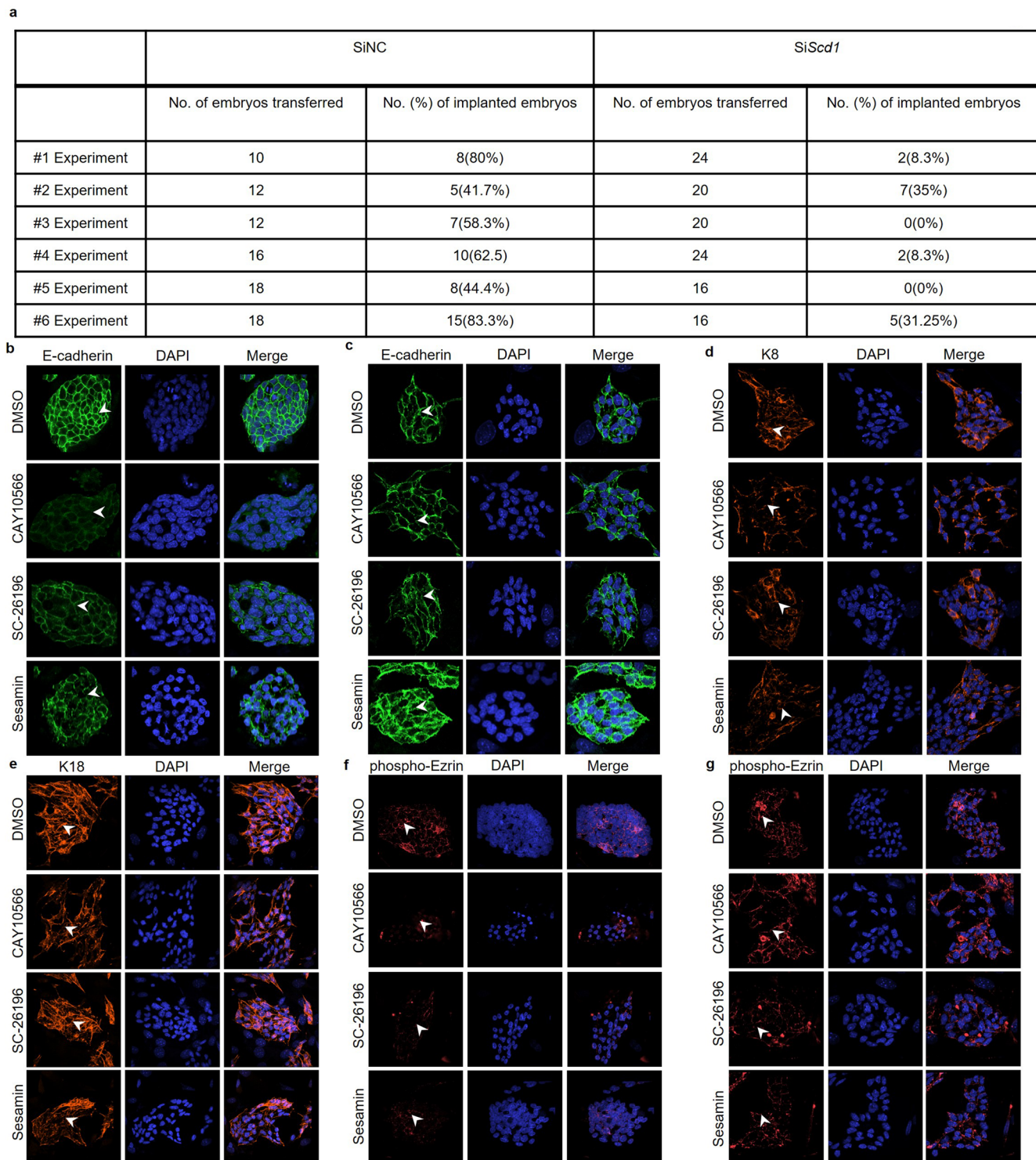
are representative of three independent experiments. (b) FRAP analysis showing recovery after photobleaching to indicate cell membrane fluidity in 3.5 d.p.c embryos treated with DMSO-, CAY10566- or CAY10566 plus oleic acid. The images shown are representative of three independent experiments.



Extended Data Fig. 8 | See next page for caption.

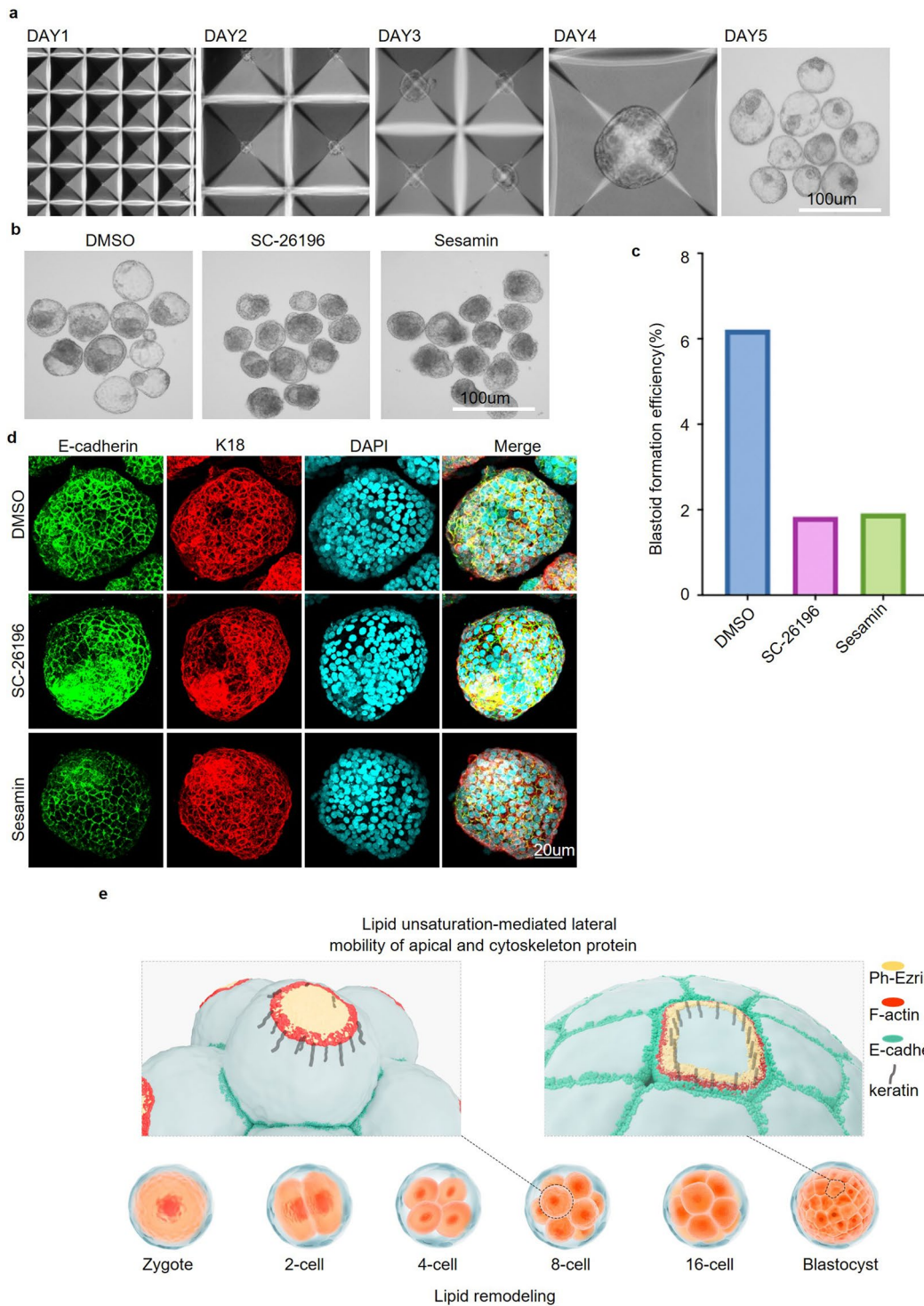
**Extended Data Fig. 8 | The desaturase SCD1 contributes to cytoskeleton organization and apical domain formation in eight-cell-to-blastocyst development.** (a) Immunofluorescence of K18 and CDX2 showing their location in 3.5 d.p.c blastocyst embryos treated with DMSO-, CAY10566- or CAY10566 plus oleic acid; the images shown are representative of one (for K18) and two (for CDX2) independent experiments. (b-d) Quantification of fluorescence intensity of the cell-cell boundary (b), cell number per embryo (c) and CDX2 intensity (d) of 3.5 d.p.c blastocyst embryos treated with DMSO-, CAY10566- or CAY10566 plus oleic acid. Each dot represents one blastocyst. Data (b, c) are from n = 5 for DMSO, n = 10 for CAY10566 and n = 6 for CAY10566 + OA-treated blastocysts, the experiment was performed for one time; data (d) are from n = 13 for DMSO, n = 20 for CAY10566 and n = 15 for CAY10566 + OA-treated blastocysts, and the experiments were repeated for two times. Data are presented as the

mean +/- s.e.m. Statistical significance was determined by two-tailed unpaired t test. Center line, median; box, 25th and 75th percentiles, whiskers, 1.5xIQR. (e) Immunofluorescence of K18 and CDX2 of 3.5 d.p.c. blastocyst embryos treated with NC, siScd1 or siScd1 plus oleic acid. The images shown are representative of two (for siScd1) and one (for siScd1 + OA) independent experiments. (f, g) Quantification of fluorescence intensity of the cell-cell boundary (f), cell number per embryo (g) of 3.5 d.p.c blastocyst embryos treated with NC, siScd1 or siScd1 plus oleic acid. Each dot represents one blastocyst. Data are from n = 17 for siNC, n = 19 for siScd1 and n = 5 for siScd1 + OA-treated blastocysts, the experiments were repeated for two (for siScd1) and one (for siScd1 + OA) times. Data are presented as the mean +/- s.e.m. Statistical significance was determined by two-tailed unpaired t test. Center line, median; box, 25th and 75th percentiles, whiskers, 1.5xIQR.



**Extended Data Fig. 9 | The desaturase SCD1 contributes to blastocyst implantation, and the desaturases for the PUFA and MUFA synthesis mediate apical-basolateral protein expression in TSCs and ESCs.** (a) A table showing the number of transferred embryos and implanted embryos with and without knocking down *Scd1*. (b) Immunofluorescence of E-cadherin in ESCs treated with DMSO, CAY10566(1uM), SC-26196(1uM), sesamin(1uM). Arrows indicate E-cadherin localization. (c) Immunofluorescence of E-cadherin in TSCs treated with DMSO, CAY10566(1uM), SC-26196(1uM), sesamin(1uM). Arrows indicate

E-cadherin localization. (d, e) Immunofluorescence of K8 and K18 in TSCs treated with DMSO, CAY10566(1uM), SC-26196(1uM), sesamin(1uM). Arrows indicate K8 and K18 localization. (f, g) Immunofluorescence of phosphorylated-ezrin(Thr567) in ESCs (f) and TSCs (g), respectively, treated with DMSO, CAY10566(1uM), SC-26196(1uM), sesamin(1uM). Arrows indicate Phospho-ezrin localization. (b-g) The images shown are representative of three independent experiments; scale bar, 30uM.



**Extended Data Fig. 10 | Desaturases for the PUFA and MUFA synthesis are required for the generation of EPS-blastoids.** (a) Representative phase-contrast images of EPSC aggregates at the indicated time to show the EPS-blastoid formation; the images shown are representative of three independent experiments. (b) Phase-contrast images of blastoid formation in the DMSO-, SC-26196 or sesamin-treated conditions; the images shown are representative of two independent experiments. (c) Quantification of blastoid formation efficiency in the DMSO-, SC-26196 and sesamin-treated conditions. Data are from two independent experiments. (d) Immunofluorescence of E-cadherin

and K18 localization in the blastoids treated with DMSO-, SC-26196 and sesamin; the images shown are representative of two independent experiments. (e) A schematic to show apical-basal polarity establishment, lateral expansion of apical domain protein phospho-ezrin and cytoskeleton proteins F-actin and Keratin, and the zippering process to seal the blastocyst embryo along the cell-cell junction during the eight-cell-to-blastocyst embryo development. The desaturase SCD1-mediated lipid unsaturation, membrane fluidity and cytoskeleton dynamics are required for these processes to take place in order to support successful blastocyst implantation in the uterus.

## Reporting Summary

Nature Portfolio wishes to improve the reproducibility of the work that we publish. This form provides structure for consistency and transparency in reporting. For further information on Nature Portfolio policies, see our [Editorial Policies](#) and the [Editorial Policy Checklist](#).

### Statistics

For all statistical analyses, confirm that the following items are present in the figure legend, table legend, main text, or Methods section.

n/a Confirmed

- The exact sample size ( $n$ ) for each experimental group/condition, given as a discrete number and unit of measurement
- A statement on whether measurements were taken from distinct samples or whether the same sample was measured repeatedly
- The statistical test(s) used AND whether they are one- or two-sided  
*Only common tests should be described solely by name; describe more complex techniques in the Methods section.*
- A description of all covariates tested
- A description of any assumptions or corrections, such as tests of normality and adjustment for multiple comparisons
- A full description of the statistical parameters including central tendency (e.g. means) or other basic estimates (e.g. regression coefficient) AND variation (e.g. standard deviation) or associated estimates of uncertainty (e.g. confidence intervals)
- For null hypothesis testing, the test statistic (e.g.  $F$ ,  $t$ ,  $r$ ) with confidence intervals, effect sizes, degrees of freedom and  $P$  value noted  
*Give P values as exact values whenever suitable.*
- For Bayesian analysis, information on the choice of priors and Markov chain Monte Carlo settings
- For hierarchical and complex designs, identification of the appropriate level for tests and full reporting of outcomes
- Estimates of effect sizes (e.g. Cohen's  $d$ , Pearson's  $r$ ), indicating how they were calculated

*Our web collection on [statistics for biologists](#) contains articles on many of the points above.*

### Software and code

Policy information about [availability of computer code](#)

#### Data collection

No custom software was used in this study  
Sequencing was performed using illumina NovaSeq6000  
Immunofluorescence data were acquired by Olympus FV3000 microscope  
Lipidomic analysis were performed by using a Shimadzu UPLC system connected to a 7500 Qtrap system (SCIEX)

#### Data analysis

Immunofluorescence data were visualized by Imaris9.0.1, ImageJ version 2.1.0/1.53c and GraphPad software version 9.0.0 (86)  
Lipidomic and Sequencing were analyzed as described in the Methods section, Software were also included as below:  
fastp v0.23.2  
STAR v.2.7.10a  
featureCounts v2.0.1  
R package DESeq v1.32.0

For manuscripts utilizing custom algorithms or software that are central to the research but not yet described in published literature, software must be made available to editors and reviewers. We strongly encourage code deposition in a community repository (e.g. GitHub). See the Nature Portfolio [guidelines for submitting code & software](#) for further information.

## Data

Policy information about [availability of data](#)

All manuscripts must include a [data availability statement](#). This statement should provide the following information, where applicable:

- Accession codes, unique identifiers, or web links for publicly available datasets
- A description of any restrictions on data availability
- For clinical datasets or third party data, please ensure that the statement adheres to our [policy](#)

The sequencing datasets have been deposited in the Gene Expression Omnibus (GEO) under the accession code of GSE213782. Source data are provided with this study.

## Research involving human participants, their data, or biological material

Policy information about studies with [human participants or human data](#). See also policy information about [sex, gender \(identity/presentation\), and sexual orientation](#) and [race, ethnicity and racism](#).

Reporting on sex and gender	No sex and gender were considered in this study design. No sex and/or gender was determined based on self-reporting or assigned and methods used. No sex- and gender-based analyses were performed.
Reporting on race, ethnicity, or other socially relevant groupings	No socially constructed or socially relevant categorization variable(s) used in our manuscript.
Population characteristics	The embryos used in this study were donated by 34 couples whose average age of the female donors was 31, and the male donor was 38 years old.
Recruitment	The couples who had successfully given birth to healthy offspring through in vitro fertilization treatment voluntarily donated excess embryos after received proper counseling regarding the research objective, the implications of their donation, and potential risks involved. No bias self-selection were presented.
Ethics oversight	The Reproductive Medicine Ethics Committee of Shengjing Hospital approved this study (Research License 2022PS004F), the research also followed the guidelines of International Society for Stem Cell Research (ISSCR) and was regularly reviewed by The Reproductive Medicine Ethics Committee of Shengjing Hospital.

Note that full information on the approval of the study protocol must also be provided in the manuscript.

## Field-specific reporting

Please select the one below that is the best fit for your research. If you are not sure, read the appropriate sections before making your selection.

Life sciences

Behavioural & social sciences

Ecological, evolutionary & environmental sciences

For a reference copy of the document with all sections, see [nature.com/documents/nr-reporting-summary-flat.pdf](https://nature.com/documents/nr-reporting-summary-flat.pdf)

## Life sciences study design

All studies must disclose on these points even when the disclosure is negative.

Sample size	No statistical method was used to pre-determine sample size. For lipidomic analysis, four to seven biological replicates, each with 120 embryos for the stages of Oocyte, Zygote and two-cell embryos, and three to five biological replicates with 120 embryos for the stages of four-cell, eight-cell and blastocyst embryos were used in this study according to our previous publication (Zhao et al; Nature Metabolism). Four biological replicates each with 30 embryos for human embryos according to the volume ratio between human and mouse. Three biological replicates were performed for RNA-seq.
Data exclusions	No data were excluded from the analysis.
Replication	3-7 replications were used in the lipidomic study. Replication of lipidomic analysis was visualized by heatmap and PCA plots, as shown in each figure and figure legends. Immunofluorescence was performed two to three times, and similar observation was found in each replicate. One representative data was shown in the figures, and the numbers of embryo and replicate were shown in figure and figure legends. Replication of sequencing data was confirmed by correlation between replicates.
Randomization	Experimental materials were not randomly allocated for lipidomic analysis, RNA-Seq, etc. Most comparisons were performed between control and experimental groups.
Blinding	The authors were not blinded to group allocation during sample collection or analysis.

# Reporting for specific materials, systems and methods

We require information from authors about some types of materials, experimental systems and methods used in many studies. Here, indicate whether each material, system or method listed is relevant to your study. If you are not sure if a list item applies to your research, read the appropriate section before selecting a response.

Materials & experimental systems		Methods	
n/a	Involved in the study	n/a	Involved in the study
<input type="checkbox"/>	<input checked="" type="checkbox"/> Antibodies	<input checked="" type="checkbox"/>	<input type="checkbox"/> ChIP-seq
<input type="checkbox"/>	<input checked="" type="checkbox"/> Eukaryotic cell lines	<input checked="" type="checkbox"/>	<input type="checkbox"/> Flow cytometry
<input checked="" type="checkbox"/>	<input type="checkbox"/> Palaeontology and archaeology	<input checked="" type="checkbox"/>	<input type="checkbox"/> MRI-based neuroimaging
<input type="checkbox"/>	<input checked="" type="checkbox"/> Animals and other organisms		
<input type="checkbox"/>	<input checked="" type="checkbox"/> Clinical data		
<input checked="" type="checkbox"/>	<input type="checkbox"/> Dual use research of concern		
<input checked="" type="checkbox"/>	<input type="checkbox"/> Plants		

## Antibodies

Antibodies used	Keratin8 (DSHB, TROMA-I) ;Keratin 18 (Sigma, SAB4501665);Nanog (R & D,AF2729);CDX2(Biogenex, AM392-5M);aPKC (Santa Cruz,17781);E-cadherin (Sigma, U3254); Ezrin (Cell Signaling Technology, 3145S); Phosphorylated-Ezrin (Cell Signaling Technology, 3726T); YAP (Cell Signaling Technology, 8418S). Secondary antibody Alexa Fluor®647 (abcam, ab150075) and Alexa Fluor® 488 (abcam, ab150061)
Validation	<p>Keratin 8 antibody : <a href="https://dshb.biology.uiowa.edu/TROMA-I">https://dshb.biology.uiowa.edu/TROMA-I</a>;</p> <p>Keratin 18 antibody : <a href="https://www.sigmaaldrich.cn/CN/zh/product/sigma/sab4501665">https://www.sigmaaldrich.cn/CN/zh/product/sigma/sab4501665</a>;</p> <p>Nanog antibody:<a href="https://www.rndsystems.com/cn/products/mouse-nanog-antibody_af2729">https://www.rndsystems.com/cn/products/mouse-nanog-antibody_af2729</a>;</p> <p>CDX2 antibody: <a href="http://store.biogenex.com/us/anti-cdx-2-clone-cdx2-130.html">http://store.biogenex.com/us/anti-cdx-2-clone-cdx2-130.html</a>;</p> <p>aPKC antibody: <a href="https://www.scbt.com/zh/p/pkc-zeta-antibody-h-1?requestFrom=search">https://www.scbt.com/zh/p/pkc-zeta-antibody-h-1?requestFrom=search</a>;</p> <p>E-cadherin antibody: <a href="https://www.sigmaaldrich.cn/CN/zh/product/sigma/u3254">https://www.sigmaaldrich.cn/CN/zh/product/sigma/u3254</a>;</p> <p>Ezrin antibody: <a href="https://www.cellsignal.cn/products/primary-antibodies/ezrin-antibody/3145?site-search-type=Products&amp;N=4294956287&amp;Ntt=3145s&amp;fromPage=plp&amp;_requestid=6008623">https://www.cellsignal.cn/products/primary-antibodies/ezrin-antibody/3145?site-search-type=Products&amp;N=4294956287&amp;Ntt=3145s&amp;fromPage=plp&amp;_requestid=6008623</a>;</p> <p>Phosphorylated-Ezrin antibody: <a href="https://www.cellsignal.cn/products/primary-antibodies/phospho-ezrin-thr567-radixin-thr564-moesin-thr558-48g2-rabbit-mab/3726?site-search-type=Products&amp;N=4294956287&amp;Ntt=3726t&amp;fromPage=plp&amp;_requestid=6008738">https://www.cellsignal.cn/products/primary-antibodies/phospho-ezrin-thr567-radixin-thr564-moesin-thr558-48g2-rabbit-mab/3726?site-search-type=Products&amp;N=4294956287&amp;Ntt=3726t&amp;fromPage=plp&amp;_requestid=6008738</a>;</p> <p>YAP antibody: <a href="https://www.cellsignal.cn/products/primary-antibodies/yap-taz-d24e4-rabbit-mab/8418?site-search-type=Products&amp;N=4294956287&amp;Ntt=8418s&amp;fromPage=plp&amp;_requestid=6008837">https://www.cellsignal.cn/products/primary-antibodies/yap-taz-d24e4-rabbit-mab/8418?site-search-type=Products&amp;N=4294956287&amp;Ntt=8418s&amp;fromPage=plp&amp;_requestid=6008837</a>;</p>

## Eukaryotic cell lines

Policy information about <a href="#">cell lines and Sex and Gender in Research</a>	
Cell line source(s)	E14 ESCs were gifts from George Q. Daley's lab at Harvard Medical Schoo, USA; TSCs were gifts from Dr. Junfeng Ji Lab at Zhejiang University School of Medicine, China.
Authentication	For ES cell lines, we performed immunofluorescence staining of OCT4 and NANOG, and RT-qPCR of marker gene Pou5f1 and Nanog, and they are highly expressed indicating these are authentic cells.
Mycoplasma contamination	we regularly perform mycoplasma tests and cells used in this study are negative for mycoplasma contamination.
Commonly misidentified lines (See <a href="#">ICLAC</a> register)	No commonly misidentified cell lines were used.

## Animals and other research organisms

Policy information about <a href="#">studies involving animals; ARRIVE guidelines</a> recommended for reporting animal research, and <a href="#">Sex and Gender in Research</a>	
Laboratory animals	All animal maintenance and experimental procedures used in this study were performed in accordance with Animal Research Committee guidelines of Zhejiang University (Research Licence ZJU20230458), Hangzhou, China. 4-6 weeks C57BL/6 female mice, 8 weeks C57BL/6 male mice and 8 weeks DBA male mice were purchased from SLAC Animal, Shanghai, China. All mice had free access to food and water maintained in an environment at 22–26°C with 50–70% humidity on a 12/12h light/dark cycle.
Wild animals	No wild animals were used in this study.
Reporting on sex	No sex-based analysis and no finding related with sex in this study.

Field-collected samples	No field-collected samples were used in this study.
Ethics oversight	All animal experiments and study protocols were approved by the Animal Research Committee guidelines of Zhejiang University, Hangzhou, China.

Note that full information on the approval of the study protocol must also be provided in the manuscript.

## Clinical data

Policy information about [clinical studies](#)

All manuscripts should comply with the ICMJE [guidelines for publication of clinical research](#) and a completed [CONSORT checklist](#) must be included with all submissions.

Clinical trial registration	The Reproductive Medicine Ethics Committee of Shengjing Hospital approved this study (Research License 2022PS004F).
Study protocol	The embryos thawing protocol, collection process and methods for lipidome are provided in the Methods section.
Data collection	The human embryos were collected at Center of Reproductive Medicine, Shengjing Hospital of China, the collection time is around half a year, all the embryos were collected according to the protocol in Methods section.
Outcomes	Four biological replicates each with 30 embryos for human embryos according to the volume ratio between human and mouse according to our previous publication (Zhao et al; Nature Metabolism), and the outcome was visualized by heatmap and PCA plots.

## Plants

Seed stocks	<i>Report on the source of all seed stocks or other plant material used. If applicable, state the seed stock centre and catalogue number. If plant specimens were collected from the field, describe the collection location, date and sampling procedures.</i>
Novel plant genotypes	<i>Describe the methods by which all novel plant genotypes were produced. This includes those generated by transgenic approaches, gene editing, chemical/radiation-based mutagenesis and hybridization. For transgenic lines, describe the transformation method, the number of independent lines analyzed and the generation upon which experiments were performed. For gene-edited lines, describe the editor used, the endogenous sequence targeted for editing, the targeting guide RNA sequence (if applicable) and how the editor was applied.</i>
Authentication	<i>Describe any authentication procedures for each seed stock used or novel genotype generated. Describe any experiments used to assess the effect of a mutation and, where applicable, how potential secondary effects (e.g. second site T-DNA insertions, mosaicism, off-target gene editing) were examined.</i>